Published OnlineFirst February 18, 2019; DOI: 10.1158/2159-8290.CD-17-1444

RESEARCH ARTICLE

BCL6 Evolved to Enable Stress Tolerance in Vertebrates and Is Broadly Required by Cancer Cells to Adapt to Stress

Tharu M. Fernando[1,2], Rossella Marullo[1], Benet Pera Gresely[1], Jude M. Phillip[1], Shao Ning Yang[1], Geoffrey Lundell-Smith[3], Ingrid Torregroza[4], Haelee Ahn[1], Todd Evans[4], Balázs Győrffy[5,6], Gilbert G. Privé[3,7], Masayuki Hirano[8], Ari M. Melnick[1,2], and Leandro Cerchietti[1]

ABSTRACT Several lines of evidence link the canonical oncogene BCL6 to stress response. Here we demonstrate that BCL6 evolved in vertebrates as a component of the HSF1-driven stress response, which has been co-opted by the immune system to support germinal center formation and may have been decisive in the convergent evolution of humoral immunity in jawless and jawed vertebrates. We find that the highly conserved BTB corepressor binding site of BCL6 mediates stress adaptation across vertebrates. We demonstrate that pan-cancer cells hijack this stress tolerance mechanism to aberrantly express BCL6. Targeting the BCL6 BTB domain in cancer cells induces apoptosis and increases susceptibility to repeated doses of cytotoxic therapy. The chemosensitization effect upon BCL6 BTB inhibition is dependent on the derepression of *TOX*, implicating modulation of DNA repair as a downstream mechanism. Collectively, these data suggest a form of adaptive nononcogene addiction rooted in the natural selection of BCL6 during vertebrate evolution.

SIGNIFICANCE: We demonstrate that HSF1 drives BCL6 expression to enable stress tolerance in vertebrates. We identify an HSF1–BCL6–TOX stress axis that is required by cancer cells to tolerate exposure to cytotoxic agents and points toward BCL6-targeted therapy as a way to more effectively kill a wide variety of solid tumors.

[1]Division of Hematology and Oncology, Department of Medicine, Weill Cornell Medicine, New York, New York. [2]Department of Pharmacology, Weill Cornell Medicine, New York, New York. [3]Department of Biochemistry, University of Toronto, Toronto, Ontario, Canada. [4]Department of Surgery, Weill Cornell Medicine, New York, New York. [5]MTA TTK Lendület Cancer Biomarker Research Group, Institute of Enzymology, Budapest, Hungary. [6]Semmelweis University 2nd Department of Pediatrics, Budapest, Hungary. [7]Princess Margaret Cancer Centre, Toronto, Ontario, Canada. [8]Emory Vaccine Center and Department of Pathology and Laboratory Medicine, Emory University, Atlanta, Georgia.

Note: Supplementary data for this article are available at Cancer Discovery Online (http://cancerdiscovery.aacrjournals.org/).

T.M. Fernando and R. Marullo contributed equally to this article.

Current address for T.M. Fernando: Discovery Oncology, Genentech, South San Francisco, California.

Corresponding Authors: Ari M. Melnick, Weill Cornell Medicine, Meyer Cancer Center, 413 E 69th Street, New York, NY 10021. Phone: 646-962-7502; E-mail: amm2014@med.cornell.edu; and Leandro Cerchietti, Weill Cornell Medicine, 1300 York Avenue, C-620B, New York, NY 10065. Phone: 212-746-7649; E-mail: lec2010@med.cornell.edu

doi: 10.1158/2159-8290.CD-17-1444

Published OnlineFirst February 18, 2019; DOI: 10.1158/2159-8290.CD-17-1444

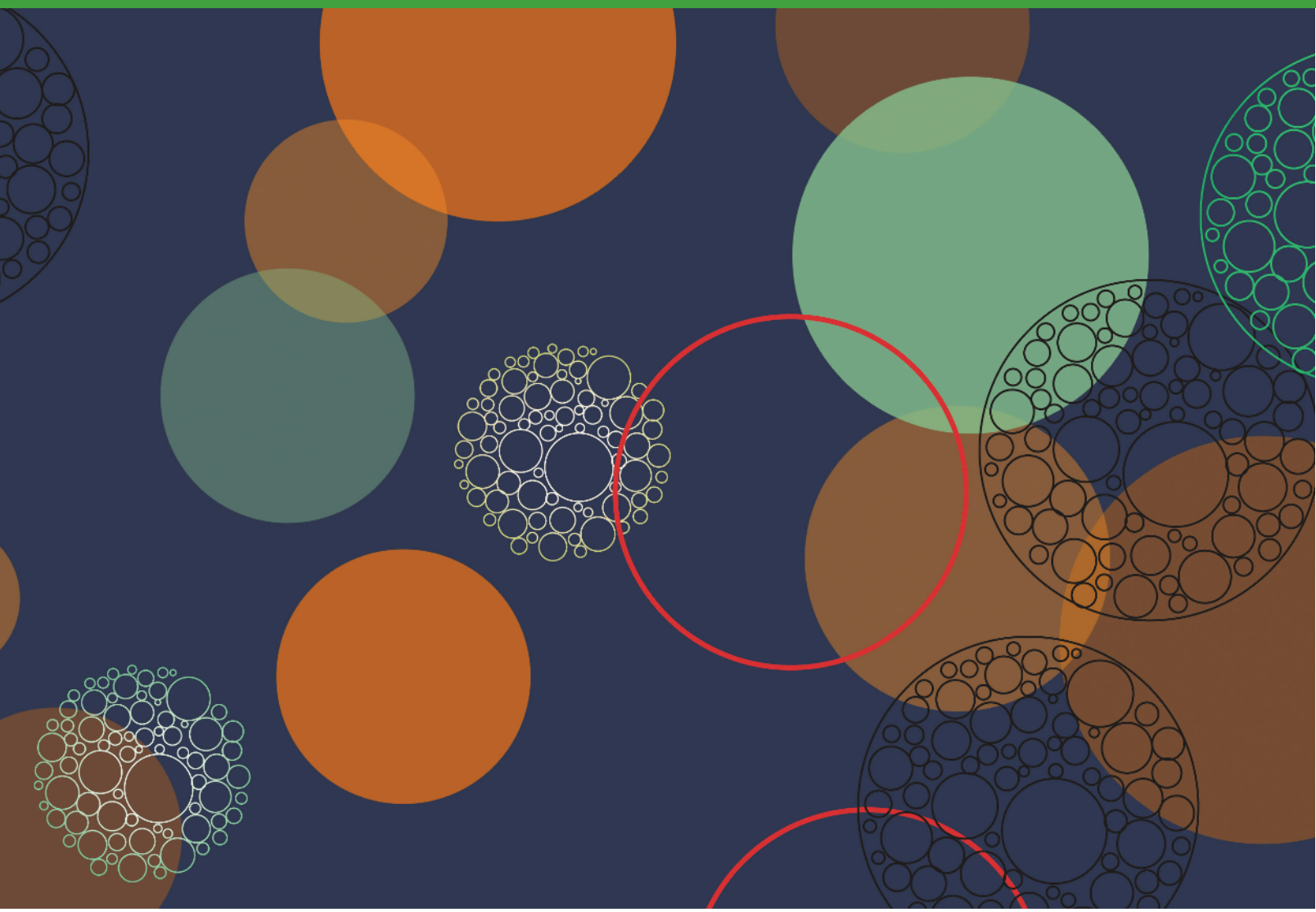

INTRODUCTION

B-cell lymphoma 6 (*BCL6*) is an oncogene in diffuse large B-cell lymphomas (DLBCL) where it is frequently expressed constitutively due to chromosomal translocations or other mutations that enhance its expression or functionality (1). Because BCL6 is also critical for germinal center (GC) B cells, which are the cell of origin of DLBCLs, it has long been thought of as a lymphoma-specific oncogene. However, recent reports have implicated BCL6 in solid tumors such as breast cancer, lung cancer, and glioblastoma (2–4), and data from The Cancer Genome Atlas (TCGA) demonstrate genomic amplification of the *BCL6* locus in certain solid tumors. Yet beyond these genetic lesions, BCL6 is expressed in many solid tumors even though it is not necessarily linked to the development of those tissues.

These findings led us to wonder how BCL6 is linked to solid tumors of distinct lineages. In the physiologic context of the GC reaction, BCL6 is required to maintain the proliferation and survival of GC B cells, which tolerate significant stress linked to their rapid proliferative rate, tolerance of somatic hypermutation, and oxidative stress (5–7). BCL6 protein expression in GC-derived lymphoma cells requires the stress chaperone heat shock protein 90 (HSP90), and BCL6 represses its target genes in lymphoma cells using HSP90 as a corepressor protein (8). Because a commonality among tumors is their dependency on stress response pathways to maintain their proliferation and survival, we postulated that BCL6 expression might be linked in some way to stress responses in solid tumors.

Heat shock factor 1 (HSF1) is the master regulator of stress response, governing the expression of HSPs and other stress proteins (9). Because HSF1 contributes to maintaining homeostasis after exposure to various stressors, it has been implicated in cellular adaptation to the malignant phenotype (10). Increased HSF1 expression has been found in several tumor types and HSF1 depletion results in decreased cell viability and chemosensitization (11–16). Furthermore, HSF1 is required for tumorigenesis and transformation by a number of oncogenes including *RAS, PDGFB*, and *HER2* (15, 17–20). Although HSF1 is not a classic oncogene, HSF1 governs a broad network of signaling pathways to support

Published OnlineFirst February 18, 2019; DOI: 10.1158/2159-8290.CD-17-1444

the tumorigenic environment, and the activation of its cancer program is associated with disease progression and predicts poor prognosis in patients with cancer (21–23).

HSF1 is expressed ubiquitously but is present in its inactive monomeric form in unstressed cells (9). After exposure to conditions that cause proteotoxic stress such as heat shock, HSF1 becomes activated, trimerizes, and shuttles to the nucleus where it binds to many stress-related target genes such as HSP90 and HSP70. HSF1 and its isoforms are the primary regulators of stress-inducible expression in eukaryotic cells. Tissues from *Hsf1*-deficient mice have normal basal expression of HSPs but lack inducible expression in response to stresses (24, 25).

Taken together, these considerations led us to hypothesize that HSF1 and BCL6 might be functionally linked. Our data show that indeed *BCL6* is a direct HSF1 target gene in stress response, and in doing so reveal an unexpected link between vertebrate development, convergent evolution of the humoral immune response in different vertebrate organisms, and most critically the rationale for translating BCL6-targeted therapy as a more specific approach to inhibit stress pathways across a broad range of human tumors.

RESULTS

BCL6 Is Widely Coexpressed with *HSF1* and Associated with Unfavorable Clinical Outcome in Solid Tumors

Recent reports have shown that BCL6 is often expressed in solid tumor cell lines that are not from the B-cell lineage (2–4). Indeed, we examined gene expression profiles collected by TCGA and found that *BCL6* is frequently overexpressed in many solid tumors including breast, lung, head and neck, esophageal, ovarian, and uterine cancers (Supplementary Fig. S1A and S1B). Furthermore, high *BCL6* transcript expression is associated with decreased progression-free survival (PFS) in at least three common aggressive cancer types: triple-negative breast cancer (TNBC), non–small cell lung cancer (NSCLC) adenocarcinoma subtype, and gastric adenocarcinoma (Fig. 1A–C, left). The HRs (95% CI) were 1.74 (1.05–2.87), 2.53 (1.94–3.30), and 1.77 (1.46–2.06) for TNBC, NSCLC, and gastric adenocarcinoma, respectively (Fig. 1A–C, left). The association of *BCL6* expression with these clinically aggressive tumors might be connected to cellular stress responses. We thus analyzed the expression of the master transcriptional regulator of the stress response, HSF1, in the same cohorts and found that high *HSF1* transcript expression is also associated with decreased PFS in these tumors with an HR of 1.46 (0.95–2.23), 1.90 (1.51–2.40), and 1.64 (1.38–1.99) for TNBC, NSCLC, and gastric adenocarcinoma, respectively (Fig. 1A–C, middle). Considering a potential link between stress response and BCL6, we hypothesized that the patients who have poor prognosis associated with high *BCL6* expression must be the same patients with high *HSF1* expression. Indeed, *BCL6* expression was significantly correlated with *HSF1* expression (Supplementary Fig. S1C). Moreover, separating patients based on high expression of both *HSF1* and *BCL6* and low expression of both genes produced even stronger HRs between patients, suggesting an additive effect of the two genes on PFS (Fig. 1A–C, right). This led us to wonder whether there could be a functional link between HSF1 and BCL6.

BCL6 Is a Direct HSF1 Target Gene

To determine whether *BCL6* is a direct HSF1 target gene, we examined the *BCL6* promoter region and identified three consensus HSF1-binding sites [heat shock element (HSE); Supplementary Fig. S2A]. We tested whether HSF1 could bind these HSEs by designing and performing AlphaLisa assays using wild-type and mutant *BCL6* HSE DNA templates and recombinant constitutively active HSF1 (Supplementary Fig. S2B). HSF1 exhibited significant sequence-specific and concentration-dependent binding to all three HSEs as compared with the negative control mutant templates (Supplementary Fig. S2C). HSF1-binding affinity depends on nucleotide sequence, density, and spacing of HSE sites. We measured HSF1-binding affinity to HSE sites from *BCL6* (HSE2) and the high-affinity target *HSPA1A* using a fluorescence polarization assay with recombinant constitutively active HSF1 and fluorescent HSE probes (Supplementary Fig. S2D). We found that HSF1 binds with 7.4 nmol/L affinity to *HSPA1A* and with 124 nmol/L affinity to *BCL6* (Supplementary Fig. S2E). To determine the functional consequence of this binding to *BCL6* expression, we subjected anesthetized $Hsf1^{+/+}$ and $Hsf1^{+/-}$ mice to mild heat shock and examined the abundance of *Bcl6* transcripts in brain, kidney, and liver. Heat shock induced *Bcl6* expression in these tissues, but this effect was significantly blunted in $Hsf1^{+/-}$ mice (Fig. 1D; Supplementary Fig. S2F). To demonstrate that *BCL6* upregulation is the consequence of the transcriptional activity of HSF1, we heat shocked fibroblasts and analyzed nascent *BCL6* transcripts. We found that heat shock induced *BCL6* nascent transcripts and that this effect was significantly diminished by HSF1 depletion ($P < 0.01$; Fig. 1E). These data indicate that HSF1 transcriptionally regulates the expression of *BCL6* in non–B-cell lineage tissues in response to stress.

We then investigated the functional link between HSF1 and BCL6 in TNBC (MDA-MB-231, MDA-MB-468), NSCLC (NCI-H460, NCI-H1299), and gastric adenocarcinoma (Hs 746T, TMK-1) cell lines, all of which express HSF1 and BCL6. We performed QChIP experiments using HSF1 antibodies

Figure 1. Tumor cells aberrantly express *BCL6* in an HSF1-dependent manner. **A–C,** Kaplan–Meier curves of progression-free survival of patients with triple-negative breast cancer (**A**), lung adenocarcinoma (**B**), or gastric cancer (**C**) stratified by *BCL6*, *HSF1*, or *BCL6* and *HSF1* expression. *n*, number of patients. **D,** *Bcl6* mRNA in heat-shocked tissues of $Hsf1^{+/+}$ and $Hsf1^{+/-}$ mice ($n = 3$ mice per genotype). **E,** Nascent *BCL6* mRNA in heat-shocked normal human adult fibroblasts transfected with nontargeting (siNT) or *HSF1* siRNAs (si*HSF1*) with accompanying immunoblot for HSF1 (bottom; representative of three biological replicates). **F,** Enrichment of HSF1 at the *BCL6* promoter in cancer cell lines in triplicates. *, $P < 0.05$; **, $P < 0.01$ (representative of three biological replicates). **G,** *BCL6* mRNA after cell lines were transduced with control (shScr) or *HSF1*-targeting shRNAs in triplicates. *, $P < 0.05$; **, $P < 0.01$ (representative of three biological replicates). **H,** Representative colony-forming assays (left) and quantification (right) of cancer cells transduced with control (shScr), *HSF1*-targeting shRNAs, or *BCL6*-targeting shRNAs (representative of at least two biological replicates). See Supplementary Fig. S2H and S2J for immunoblots. *P* values were calculated by two-sided *t* test. Data presented as mean ± SEM.

Published OnlineFirst February 18, 2019; DOI: 10.1158/2159-8290.CD-17-1444

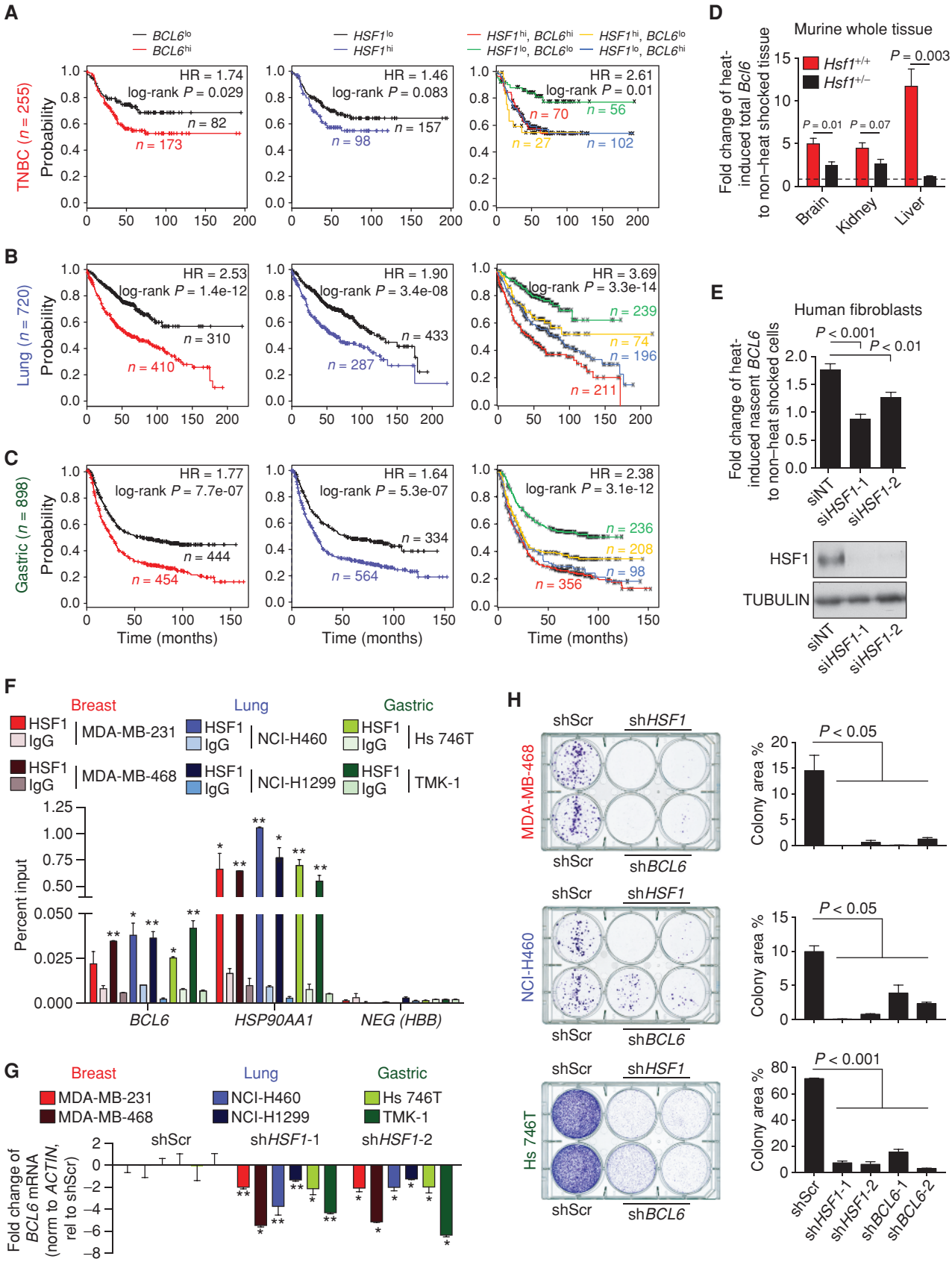

Published OnlineFirst February 18, 2019; DOI: 10.1158/2159-8290.CD-17-1444

and detected significant enrichment of HSF1 versus control antibody to the *BCL6* promoter in almost all cases (Fig. 1F). As a positive control, we found enriched HSF1 binding to the promoter of its canonical target gene *HSP90AA1*, but not a negative control region (Fig. 1F). HSF1 binding was functionally significant because knockdown using two different shRNA constructs decreased the expression of *BCL6* and *HSP90AA1* mRNAs in TNBC, NSCLC, and gastric adenocarcinoma cell lines and BCL6 protein expression (Fig. 1G; Supplementary Fig. S2G and S2H). As expected, HSF1 knockdown also caused significant impairment of colony formation by these tumor cells (Fig. 1H; Supplementary Fig. S2I). Likewise, BCL6 knockdown using two different constructs (Fig. 1H; Supplementary Fig. S2I and S2J) significantly impaired colony-forming potential in TNBC, NSCLC, and gastric adenocarcinoma cell lines ($P < 0.05$, $P < 0.05$, and $P < 0.01$, respectively), similar to HSF1 knockdown (Fig. 1H; Supplementary Fig. S2I). Taken together, these results place BCL6 downstream of HSF1 as an essential stress-related factor in solid tumor cells.

HSF1 Drives Physiologic *BCL6* Expression in GC B cells

Given that *BCL6* is induced by HSF1 in normal and malignant cells, we next investigated whether a putative HSF1–BCL6 axis was physiologically relevant to the canonical BCL6 function in the GC reaction. In normal B-cell development, BCL6 expression is absent from naïve B (NB) cells but is strongly upregulated in GC B cells (26, 27). Using QChIP assays, we observed more than a 4-fold increase in HSF1 binding at the *BCL6* promoter in purified primary human GC B cells versus NB cells (Fig. 2A). HSF1 binding was also increased at the *HSP90AA1* promoter in GC B cells relative to NB cells (Fig. 2A). We next explored whether HSF1 mediates stress-dependent transcriptional activation of *BCL6* in primary B cells. However, because HSP90 can posttranscriptionally stabilize *BCL6* mRNA (8), it was necessary to specifically determine whether heat shock and HSF1 could induce the formation of newly transcribed *BCL6* mRNA. To this end, murine splenic B cells ($B220^+$) purified from $Hsf1^{+/+}$, $Hsf1^{+/-}$, and $Hsf1^{-/-}$ mice were subjected to heat shock and enriched for nascent transcripts using ethynyl uridine capture. After heat shock, there was a 5-fold induction of nascent *Bcl6* transcripts in $Hsf1^{+/+}$ cells. In contrast, *Bcl6* transcription was significantly impaired in $Hsf1^{+/-}$ and completely abrogated in $Hsf1^{-/-}$ B cells ($P < 0.05$ for both vs. $Hsf1^{+/+}$; Fig. 2B).

The fact that *BCL6* is an HSF1 target gene in this context led us to question whether HSF1 is activated and plays a role in the development of GC B cells. The phosphorylation of HSF1 at Ser^{326} and its nuclear localization are markers of HSF1 activation (28). We therefore performed immunofluorescence studies on tissue sections of human tonsils using antibodies against BCL6 and HSF1-$pSer^{326}$. Examination of GCs revealed nuclear coexpression of these two proteins in many GC B cells (Fig. 2C). As a second line of evidence for HSF1 activation, we compared DNA-binding activity of HSF1 in nuclear lysates of primary human NB versus GC B cells using the AlphaLisa quantitative DNA-binding assay and probes corresponding to wild-type or mutant HSEs. These experiments showed significant increase in HSF1 DNA binding in GC versus NB cells ($P < 0.01$; Fig. 2D). This effect was not due to differential expression of HSF1 because protein levels were similar in NB and GC B cells (Fig. 2D). Having established that HSF1 is active in GC B cells, we wondered whether this was purely due to the high stress nature of these cells or whether immune signaling linked to the initiation of GCs might also be involved, perhaps to prepare cells to tolerate stress conditions. We therefore treated primary human NB cells with CD40 ligand, IL4, or IL21 (canonical signals known to initiate the GC reaction; refs. 29, 30) and compared HSF1-binding activity to that induced by the canonical heat shock response. All three of these signaling ligands induced a significant and similar degree of HSF1 activation as heat shock ($P < 0.01$; Fig. 2E). To further explore whether HSF1 activation within the GC precedes *BCL6* induction in GC B cells, we performed time-course experiments where mice immunized with the T cell–dependent antigen sheep red blood cells (SRBC) were sacrificed at 8 time points after immunization ranging from 48 to 250 hours postimmunization. GC B cells (marked by IHC staining of PNA) from the spleens of these animals were then examined for the presence of nuclear HSF1 and BCL6 at each time point. Fractional positivity of HSF1 and BCL6 showed that HSF1 nuclear expression reached a plateau at 72 hours after immunization, whereas BCL6 expression continued to increase until reaching its maximum expression at around 160 hours (Fig. 2F; Supplementary Fig. S3A). This suggests that HSF1 activation precedes BCL6 expression; however, the sustained increase in BCL6 despite plateauing levels of HSF1 implies that other factors may mediate further increases in BCL6.

HSF1 Expression in B Cells Is Required for Normal GC Development

$Hsf1^{-/-}$ mice were shown to exhibit defects in immunoglobulin affinity maturation, suggesting a key role in the humoral immune response (31). However, it was not known

Figure 2. B cells require HSF1-dependent BCL6 induction for optimal germinal center formation. **A,** Enrichment of HSF1 in NB and GC B cells at the *BCL6* promoter, *HSP90AA1* promoter, and a negative control *HBB* (representative of three biological replicates). **B,** Nascent *Bcl6* mRNA in heat-shocked murine $B220^+$ splenocytes of $Hsf1^{+/+}$, $Hsf1^{+/-}$, and $Hsf1^{-/-}$ mice normalized to *Hprt1* ($n = 3$ mice per genotype). **C,** Immunofluorescence of paraffin-embedded serial human tonsillar sections. **D,** AlphaLisa activity of *HSPA1A* HSE from nuclear protein of human tonsillar NB and GC B cells ($n = 5$ pooled replicates) with accompanying immunoblot for total HSF1 (right). **E,** AlphaLisa activity of the consensus *HSPA1A* HSE from nuclear protein from human splenic NBs resting (CON), heat-shocked (HS), or treated with immune stimuli ($n = 4$–7 pooled replicates). **F,** Fraction of PNA^+ $HSF1^+$ (blue) or PNA^+ $BCL6^+$ (red) cells per GC postimmunization as a function of time. Polynomial fits (solid line) of real data points (dashed line) are shown. **G–J,** Representative PNA staining (**G**), GC size (**H**), GC number (**I**), and percentage (**J**) of $Hsf1^{+/+}$ and $Hsf1^{-/-}$ mice after immunization ($n = 4$ mice per genotype). **K,** Titers of high-affinity NP-specific IgG2a from $Hsf1^{+/+}$ and $Hsf1^{-/-}$ mice after immunization with NP-CGG (mean ± SEM, $n = 4$–6 mice per genotype). **L–N,** Bone marrow chimeras generated with $CD45.1^+$ $Hsf1^{+/+}$ and $CD45.2^+$ $Hsf1^{+/+}$ or $Hsf1^{-/-}$ mice (**L**). Representative flow cytometry plot of $CD45.2^+$ GC B cells (**M**) and GC T_{FH} cells (**N**) from mice after immunization ($n = 4$–5 mice per genotype). See Supplementary Fig. S3C–S3E for chimerism and $CD45.1^+$ GC B cells and GC T_{FH} cells. **O,** BCL6 staining intensity in splenic GC B cells from $Hsf1^{+/+}$ and $Hsf1^{-/-}$ mice after immunization. *P* values were calculated by two-sided *t* test. Data presented as mean ± SEM.

Published OnlineFirst February 18, 2019; DOI: 10.1158/2159-8290.CD-17-1444

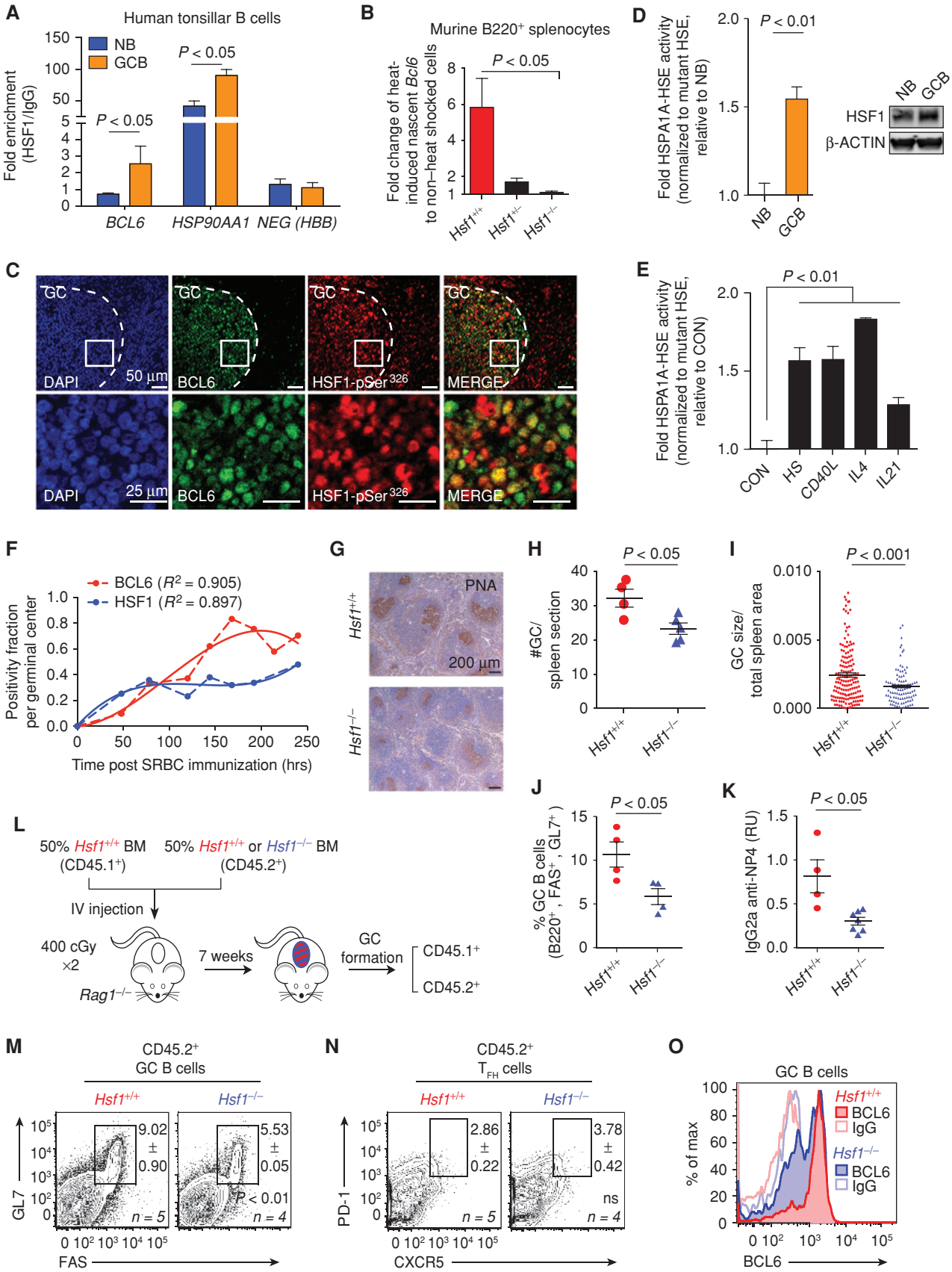

Published OnlineFirst February 18, 2019; DOI: 10.1158/2159-8290.CD-17-1444

whether HSF1 is required for the development of GC B cells or whether the affinity maturation defect was due to effects on other cell types or the microenvironment. The fact that HSF1 is active in GC B cells indicates that it is functional. But to determine whether this activity translates into phenotypic effects, we first immunized *Hsf1*$^{-/-}$ or *Hsf1*$^{+/+}$ mice with SRBC and then examined spleens for GC formation 10 days later. Staining for PNA revealed that GCs were significantly reduced in number ($P < 0.05$) as well as in surface area ($P < 0.001$; Fig. 2G–I). Likewise, flow cytometry analysis indicated a significant reduction in the fraction of GC B cells (B220$^+$, FAS$^+$, GL7$^+$) among total splenic B220$^+$ B cells ($P < 0.05$; Fig. 2J). In contrast, there was no difference in overall splenic architecture or numbers of B220$^+$ B cells in *Hsf1*$^{-/-}$ mice (Supplementary Fig. S3B). Hence the defect observed is specific to GC B cells but not total B cells. To determine whether there is indeed a defect in affinity maturation linked to this GC phenotype, we immunized *Hsf1*$^{-/-}$ or *Hsf1*$^{+/+}$ mice with the specific T cell–dependent antigen NP-CGG and then collected serum to measure high-affinity antibody titers by ELISA. *Hsf1*$^{-/-}$ mice generated significantly lower titers of high-affinity IgG2a compared with *Hsf1*$^{+/+}$ mice ($P < 0.05$, Fig. 2K).

GC formation requires intimate cooperation between B cells and T follicular helper (T_{FH}) cells (32–34). Both cell types require the presence of BCL6, and loss of function of either one abrogates GC formation. T_{FH} cells do not undergo massive proliferation or somatic hypermutation and hence do not experience the level of stress endured by GC B cells; hence, we predicted that the GC impairment phenotype was B-cell autonomous. To test this, we performed mixed chimera bone marrow transplantations using T and B cell–deficient *Rag1*$^{-/-}$ mice as recipients. *Rag1*$^{-/-}$ recipients were transplanted with CD45.1 bone marrow from *Hsf1*$^{+/+}$ mice mixed with either CD45.2 *Hsf1*$^{-/-}$ or CD45.2 *Hsf1*$^{+/+}$ cells at 50% ratio and were found to have similar engraftment (Fig. 2L; Supplementary Fig. S3C). After engraftment, GC formation was induced by immunization with SRBC, and spleens were examined 10 days later. Here, we again observed a significant 50% reduction in GC B cells (B220$^+$, FAS$^+$, GL7$^+$) from CD45.2$^+$ *Hsf1*$^{-/-}$ as compared with CD45.2$^+$ *Hsf1*$^{+/+}$ cells ($P < 0.01$; Fig. 2M) but no change in CD45.1 cells (Supplementary Fig. S3D). In marked contrast, there was no defect in T_{FH} cells (CD4$^+$, PD1$^+$, CXCR5$^+$, B220$^-$; Fig. 2N; Supplementary Fig. S3E), hence the requirement for HSF1 in GC formation was B-cell autonomous. Notably, in the remaining CD45.2$^+$ *Hsf1*$^{-/-}$ GC B cells, expression of BCL6 was generally lower than CD45.2$^+$ *Hsf1*$^{+/+}$ cells (Fig. 2O). The remaining BCL6 levels in *Hsf1*$^{-/-}$ GC B cells are likely due to other GC transcription factors that can induce BCL6 expression (35). Taken together with the activation of HSF1 downstream of GC signals (Fig. 2E), our data suggest that the described HSF1–BCL6 axis plays an important role in the formation of GCs, linked both to canonical immune signaling and stress response.

The HSF1–BCL6 Axis Is Evolutionarily Conserved

Given the conservation of HSEs in the *BCL6* promoter and its stress-induced regulation by HSF1, we postulated that BCL6 evolved as a component of the HSF1 stress response pathway. BCL6 is a member of the BTB-ZF gene family, and although members of this family are found throughout metazoan organisms, we find that BCL6 orthologs are restricted to vertebrates. Notably, jawless fish (agnathans) such as lampreys, which were the first vertebrates to evolve approximately 500 million years ago, encode a protein with >40% sequence identity to human BCL6 (Supplementary Fig. S4A) that identifies human BCL6 as the top hit in a reciprocal blast search. BCL6 is also present in all jawed vertebrates (gnathostomes), which branched off from the agnathans in the Ordovician period. To explore the HSF1–BCL6 axis across evolution, we induced heat shock in cells from mammals (humans, mice, dogs), birds (chicken), reptiles (iguana), ray-finned fish (zebrafish), and agnatha (lamprey). *BCL6* transcripts as well as two positive control heat shock genes were detected by qPCR and were significantly upregulated after heat shock in every species ($P < 0.05$, Fig. 3A; Supplementary Fig. S4B). Using Shannon entropy mapping, we observed that the BCL6 BTB domain and ZFs are the most highly conserved regions of BCL6 (Supplementary Fig. S4C). Using a polyclonal antibody against the highly conserved BCL6 BTB domain, we observed an increase in BCL6 protein abundance after heat shock in these vertebrate species ($P < 0.05$, Fig. 3B).

To determine the functional relevance of BCL6 in the canonical HSF1 stress response pathway, we assessed survival of resting B cells from *Bcl6*$^{+/+}$ or *Bcl6*$^{-/-}$ mice after heat shock (Fig. 3C). There was no significant difference in stress-induced killing between these genotypes, perhaps because *BCL6* is transcriptionally induced by HSF1 and so would not be immediately available to cells (Fig. 3C; tan bars). Postulating that HSF1 induction of *BCL6* might instead enable cells to adapt to repeated stress, we exposed *Bcl6*$^{+/+}$ B cells to sequential heat shock and found that the cells became significantly more resilient after the second stress exposure ($P = 0.003$, Fig. 3C, red bars). In striking contrast, *Bcl6*$^{-/-}$ B cells completely failed to adapt to stress (Fig. 3C). To determine whether this function is evolutionarily conserved, we performed similar experiments with zebrafish embryos using morpholino-oligonucleotide depletion of BCL6 (Supplementary Fig. S4D). Again, depletion of BCL6 abrogated adaptation to stress after the second heat shock ($P = 0.04$, Fig. 3D, red bars) but had no effect on the response to the initial stress (Fig. 3D, tan bars). These data indicate that BCL6 functions within the HSF1 program to mediate cellular adaptation to repetitive stress, a challenge faced by GC B cells and cancer cells.

Highly Conserved BCL6 BTB Domain Surface Residues Mediate Stress Adaptation Role

BCL6 mediates transcriptional repression through its BTB and RD2 domains, but we noted that only the BTB domain is highly conserved across vertebrate evolution (Supplementary Fig. S4C). The BCL6 BTB domain mediates repression by forming a "lateral groove" that is bound by a 17-residue BCL6 binding domain (BBD) from the NCOR1 and NCOR2 (SMRT) corepressors. Strikingly, the amino acids that form the BTB lateral groove corepressor-binding interface are 100% evolutionarily conserved, whereas other surface areas manifest greater variability (Fig. 4A). Likewise, the NCOR1 BBD is also highly conserved (Supplementary Fig. S5A and S5B). Because of this conservation, we predicted that the BCL6 stress adaptation function would be dependent on the BTB lateral groove but not the RD2 domain. We performed stress response experiments using B cells from mice where the endogenous *Bcl6*

Published OnlineFirst February 18, 2019; DOI: 10.1158/2159-8290.CD-17-1444

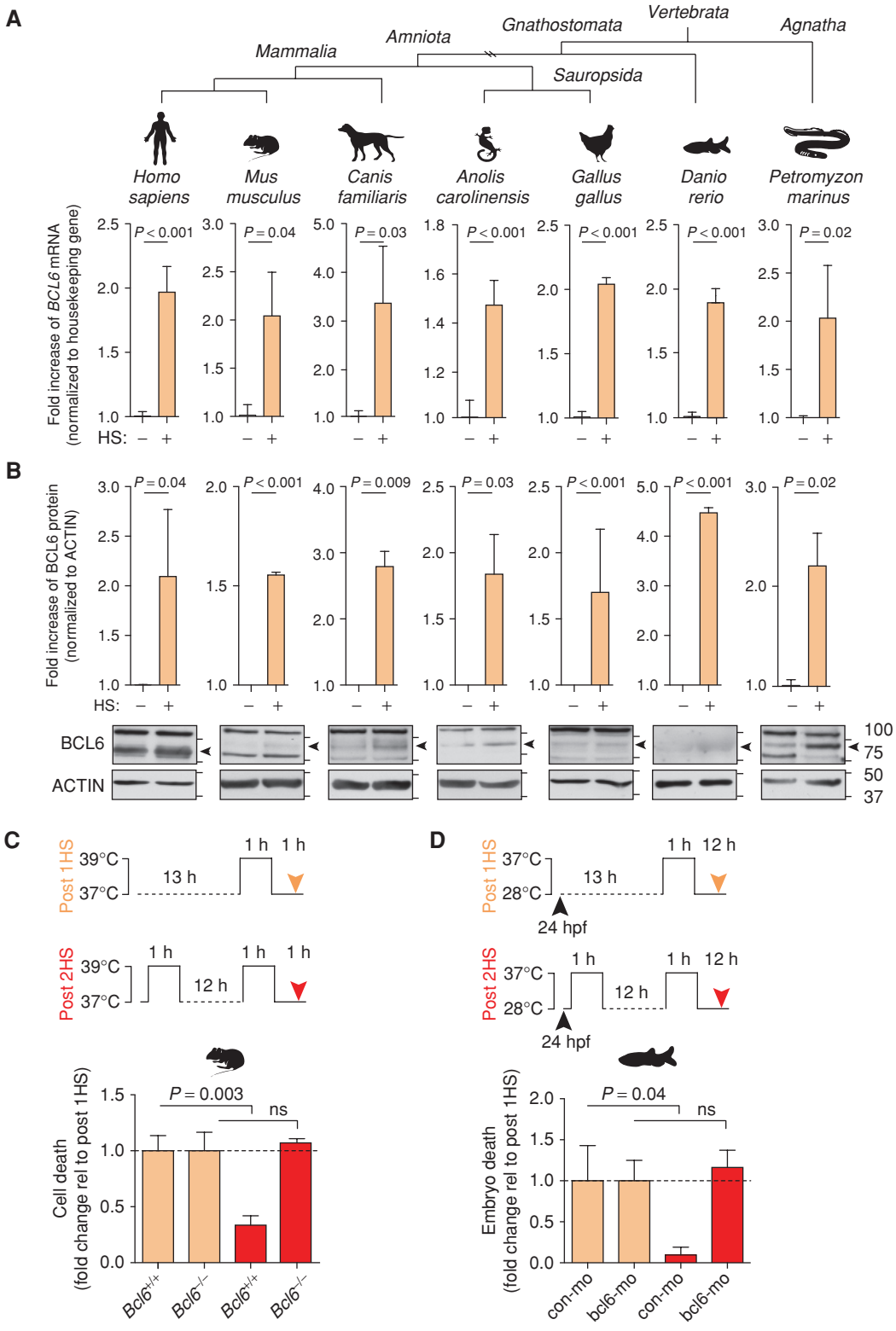

Figure 3. BCL6 is upregulated in response to stress and mediates cell adaptation to repeated stress. **A** and **B,** *BCL6* mRNA (**A**) and protein (**B**) in heat-shocked human adult fibroblasts, murine BCL1 B cells, dog Cf2Th thymocytes, iguana IgH-2 epithelial cells, chicken DT40 B cells, zebrafish embryos, and sea lamprey typhlosole tissue ($n = 3$ biological replicates). **C** and **D,** Serial stress assays where cells were heat shocked once (tan) or serially heat shocked (red). Fold change of cell death in murine B220$^+$ splenocytes from *Bcl6*$^{+/+}$ and *Bcl6*$^{-/-}$ mice ($n = 3$–5 mice per group; **C**) or zebrafish embryos injected with control or bcl6 morpholino (mo; $n = 3$ biological replicates, 75–100 embryos per experiment; **D**). See Supplementary Fig. S4D for immunoblots and qPCR of BCL6 knockdown. *P* values were calculated by two-sided *t* test. Data presented as mean ± SEM.

Published OnlineFirst February 18, 2019; DOI: 10.1158/2159-8290.CD-17-1444

locus was engineered to express a protein with point mutations in the BTB lateral groove (*Bcl6*^{BTBMUT}) or the RD2 domain (*Bcl6*^{RD2MUT}) without affecting BCL6 folding, stability, or DNA binding (36, 37). We found that whereas stress adaptation was completely abolished in *Bcl6*^{BTBMUT} cells, *Bcl6*^{RD2MUT} cells were indistinguishable from wild-type cells (Fig. 4B).

To extend this observation to non–model vertebrate species, we took advantage of a cell-penetrating decoy peptide called RI-BPI that specifically binds the BCL6 BTB lateral groove to block NCOR1/NCOR2 corepressor recruitment (38). Similar to *Bcl6*^{BTBMUT} mice, exposure to RI-BPI abrogated adaptation to stress in mouse B cells (Fig. 4B). Similar results were obtained in avian and reptile cells (Fig. 4C and D). Even in agnathans, the most distally related vertebrate class, RI-BPI specifically disrupted stress adaptation but not response to acute stress (Fig. 4E). In contrast, insect cells, which do not encode BCL6, acquired stress tolerance after serial heat shock even in the presence of RI-BPI (Fig. 4F). These data suggest that BCL6 mediates stress tolerance in vertebrates through its BTB lateral groove repressor function. Given that the lateral groove is the most

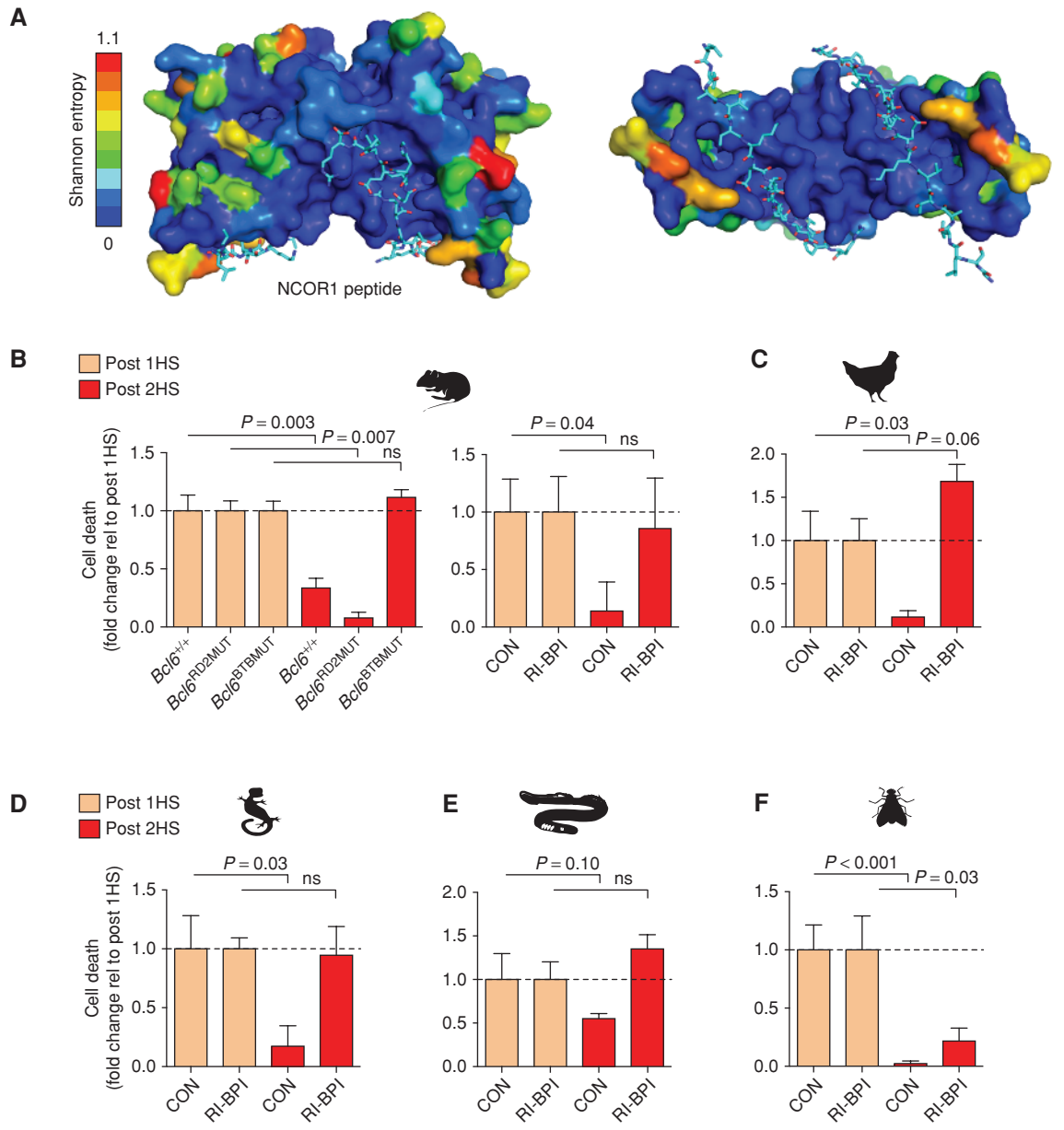

Figure 4. The lateral groove of the BCL6 BTB domain mediates cell adaptation to repeated stress. **A,** Shannon entropy values mapped onto the structure of BCL6 BTB domain. NCOR1 peptide shown in cyan. **B,** Fold change of cell death in murine B220$^+$ splenocytes from *Bcl6*$^{+/+}$, *Bcl6*^{RD2MUT}, *Bcl6*^{BTBMUT}, or *Bcl6*$^{+/+}$ mice treated with vehicle or RI-BPI that were heat shocked either once (tan) or serially heat shocked (red; $n = 3$–5 mice per group). **C–F,** Fold change of cell death in chicken DT40 B cells (**C**), iguana IgH-2 epithelial cells (**D**), sea lamprey typhlosole cells (**E**), and *Drosophila* S2 cells (**F**) treated with either vehicle (CON) or RI-BPI and heat shocked once (tan) or serially heat shocked (red; $n = 3$–6 biological replicates). *P* values were calculated by two-sided *t* test. Data presented as mean ± SEM.

Published OnlineFirst February 18, 2019; DOI: 10.1158/2159-8290.CD-17-1444

conserved BTB surface feature, it seems plausible that this stress function may explain at least in part why natural selection has maintained BCL6 throughout vertebrate evolution.

BCL6 Induces a Characteristic Gene Expression Signature during Stress Tolerance

To identify genes repressed through the BCL6 BTB domain that are required for stress adaptation, we performed RNA sequencing in *Bcl6*$^{+/+}$ and *Bcl6*^{BTBMUT} B220^{+} murine cells before and 12 hours after heat shock. Principal component analysis of these gene expression profiles readily segregated specimens based on both exposure to stress and integrity of the BTB domain (Fig. 5A). As expected, the majority of genes downregulated (absolute fold change >1.3, FDR < 0.05) after heat shock were repressed in both *Bcl6*$^{+/+}$ and *Bcl6*^{BTBMUT} cells (Fig. 5B). However, we also identified 510 genes downregulated in *Bcl6*$^{+/+}$ but not *Bcl6*^{BTBMUT} cells (Fig. 5B). These genes, which represent those that fail to be repressed by BTB-mutant BCL6, are in fact BCL6-regulated targets, as they are significantly enriched among genes that are induced by *BCL6* siRNA in B-cell lines (FDR = 0.02 and NES: 1.47; Fig. 5C). In addition, they were enriched for functional categories involved in stress response and cell cycle (Fig. 5D). Among the genes that failed to be repressed by BCL6 after heat shock in *Bcl6*^{BTBMUT} cells were *lfitm2, Npas4, Nr4a2, Prickle1, Rab34, Rasbp1*, and *Tox* (Fig. 5E). We independently confirmed specific loss of repression of most of these genes upon heat shock in B220^{+} and brain cells from *Bcl6*^{BTBMUT} mice (Fig. 5F).

Although the stress adaptation function of BCL6 is likely a consequence of the collective repression of many of its target genes, we further investigated the role of the transcription factor *TOX*, one of the most upregulated genes within the gene set enrichment analysis (GSEA) leading edge (Fig. 5E). To determine whether blocking *TOX* upregulation upon BCL6 BTB inhibition would partially rescue the stress adaptation phenotype, we exposed B220^{+} cells from *Tox*$^{-/-}$ or *Tox*$^{+/+}$ mice to RI-BPI followed by heat shock. RI-BPI decreased the stress adaptation of *Tox*$^{+/+}$ B220^{+} cells as expected, but this effect was significantly attenuated in *Tox*$^{-/-}$ B220^{+} cells (Fig. 5G), suggesting that BCL6^{BTB} repression of *TOX* contributes to stress tolerance.

HSF1-Dependent BCL6^{BTB} Repression of *TOX* Contributes to DNA Damage Tolerance in Cancer Cells

To determine whether the stress-adaptive HSF1–BCL6–TOX axis described above is also functional in tumor cells, we knocked down HSF1 in TNBC (MDA-MB-468) and NSCLC (NCI-H460) cell lines. We observed both a decrease in *BCL6* and a concomitant increase in *TOX* mRNA abundance (Fig. 6A) indicating that this regulatory loop is conserved in cancer cells. Beyond its constitutive maintenance of stress response and survival of tumor cells, HSF1 is further induced by exposure to cytotoxic drugs, an effect that facilitates emergence of drug-tolerant cells (39). To investigate whether BCL6 also follows this pattern, we exposed a panel of cancer cell lines of different histologic origin (i.e., breast, lung, gastric, bladder, and ovarian cancer) to the DNA-damaging agent doxorubicin and observed a strong positive correlation (Spearman $r = 0.777$; $P = 0.002$) between *BCL6* and *HSPA1B* induction after doxorubicin (Fig. 6B). To test whether the BCL6 BTB domain enables tolerance to DNA damage, we exposed TNBC, NSCLC, and gastric adenocarcinoma cell lines to increasing concentrations of doxorubicin and RI-BPI. We then determined the dose reduction index (DRI), a measure of the chemosensitization effect of RI-BPI. Notably, the addition of RI-BPI resulted in a favorable DRI of doxorubicin (Fig. 6C; Supplementary Fig. S6A), suggesting that the BCL6 BTB domain is critical for tolerating doxorubicin exposure. These results were independently confirmed with BCL6 knockdown (Supplementary Fig. S6B).

To determine whether this phenomenon was linked to BCL6-mediated repression of *TOX*, we perturbed the HSF1–BCL6 axis in doxorubicin-treated cell lines using *HSF1*-targeted shRNAs and RI-BPI. Although HSF1 knockdown and RI-BPI treatment by themselves both induced expression of *TOX* in doxorubicin-treated breast and lung cancer cells, the greatest induction of *TOX* was observed when combining HSF1 and BCL6 inhibition (Fig. 6D). Most strikingly, depletion of TOX from these cells (Supplementary Fig. S6C) prevented the specific small-molecule BCL6^{BTB} inhibitor FX1 (40) from inducing chemosensitization (Fig. 6E), suggesting that BCL6^{BTB}-dependent repression of *TOX* contributes to the survival of cancer cells exposed to a DNA-damaging agent.

Because TOX was shown to inhibit error-prone nonhomologous end joining (NHEJ) DNA repair in T-cell acute lymphoblastic leukemia (T-ALL; ref. 41), we hypothesized that BCL6 repression of *TOX* promotes chemotolerance by enhancing DNA repair. To test this notion, we exposed parental and TOX-silenced MDA-MB-468 and NCI-H460 cells to doxorubicin alone or in combination with the BCL6^{BTB} inhibitor FX1 and assessed DNA damage by single-cell gel electrophoresis. Neither BCL6^{BTB} inhibition nor TOX depletion affected the amount of damage induced by doxorubicin (4-hour exposure; Supplementary Fig. S6D). However, when doxorubicin was removed from the media to allow cancer cells to repair DNA damage (4-hour repair), we found that FX1 resulted in higher levels of residual DNA damage compared with doxorubicin alone (Fig. 6F). Notably, the impairment of DNA repair observed upon inhibition of the BCL6 BTB domain was entirely (MDA-MB-468) or partially (NCI-H460) rescued in TOX-silenced cells (Fig. 6F). This mechanism appears to be clinically relevant, because patients with TNBC, NSCLC, and gastric adenocarcinoma with high *BCL6* and low *TOX* expression levels have worse survival outcomes compared with patients with low *BCL6* and high *TOX* expression (Supplementary Fig. S6E). Taken together, these data suggest that the HSF1–BCL6 axis promotes tolerance toward cytotoxic drugs at least in part by repressing *TOX* and subsequently enhancing DNA repair capability in cancer cells.

Targeting the BCL6 BTB Domain Overcomes Chemotherapy Tolerance in Cancer Cells

To further validate the notion that BCL6^{BTB}-targeted therapy could be used to reverse the BCL6 stress-tolerant phenotype and sensitize solid tumors to chemotherapy, we performed additional experiments with the BCL6 small-molecule inhibitor FX1, both *in vitro* and *in vivo* (40). TNBC, NSCLC, and gastric adenocarcinoma cell lines were exposed to increasing concentrations of clinically relevant chemotherapy drugs, doxorubicin, cisplatin, paclitaxel and gemcitabine, and FX1. Like the combination of RI-BPI and doxorubicin, we found that the addition of FX1 also resulted in a favorable DRI of all cytotoxic drugs

Published OnlineFirst February 18, 2019; DOI: 10.1158/2159-8290.CD-17-1444

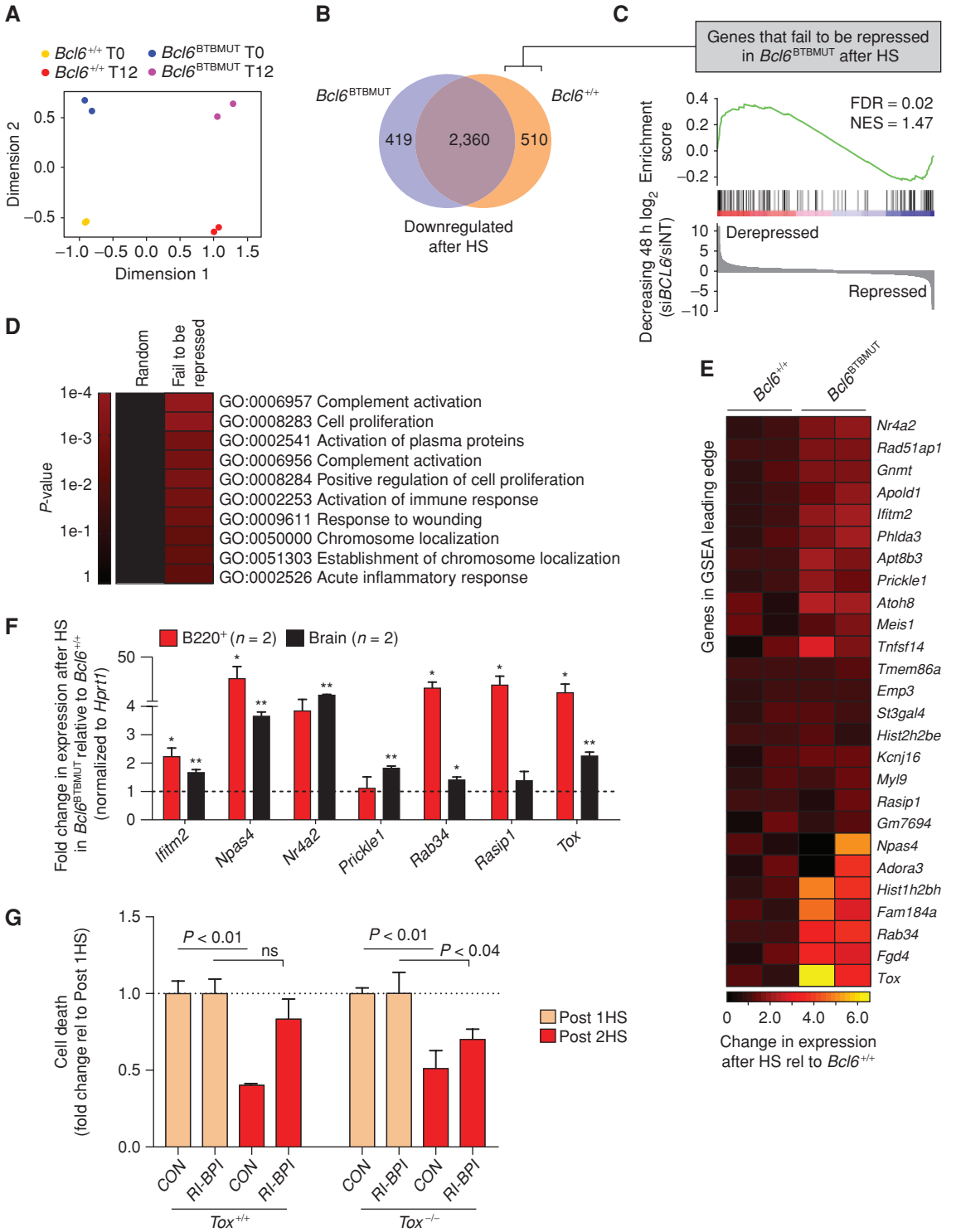

Figure 5. BCL6^{BTB}-mediated repression of *TOX* is required for cell adaptation to repeated stress. **A,** Multidimensional scaling plot of the leading biological coefficient of variation between samples using the 500 most variable genes in *Bcl6*$^{+/+}$ ($n = 2$) and *Bcl6*^{BTBMUT} ($n = 2$) B220^{+} splenocytes before (T0) and 12 hours after a single heat shock (T12). **B,** Venn diagram of genes significantly (FDR < 0.05) downregulated after heat shock that are common and unique to *Bcl6*$^{+/+}$ and *Bcl6*^{BTBMUT} B220^{+} cells. **C,** GSEA of genes that fail to be repressed in *Bcl6*^{BTBMUT} B220^{+} splenocytes after heat shock with gene expression changes in DLBCL cells after BCL6 knockdown. **D,** Gene ontology analysis of genes that fail to be repressed in *Bcl6*^{BTBMUT} B220^{+} splenocytes after heat shock. Enrichment was measured using hypergeometric *P* values. **E,** Heat map of gene expression changes after heat shock of the GSEA leading edge genes described in **C**. **F,** Gene expression changes after heat shock in B220^{+} splenocytes and brain tissue of *Bcl6*^{BTBMUT} relative to *Bcl6*$^{+/+}$ mice (mean ± SEM, $n = 2$ mice per group). *, $P < 0.05$; **, $P < 0.01$. **G,** Fold change of cell death in *Tox*$^{+/+}$ and *Tox*$^{-/-}$ B220^{+} splenocytes treated with RI-BPI and serially heat shocked (mean ± SEM, $n = 2$–4 mice per group). *P* values were calculated by two-sided *t* test unless otherwise stated.

Published OnlineFirst February 18, 2019; DOI: 10.1158/2159-8290.CD-17-1444

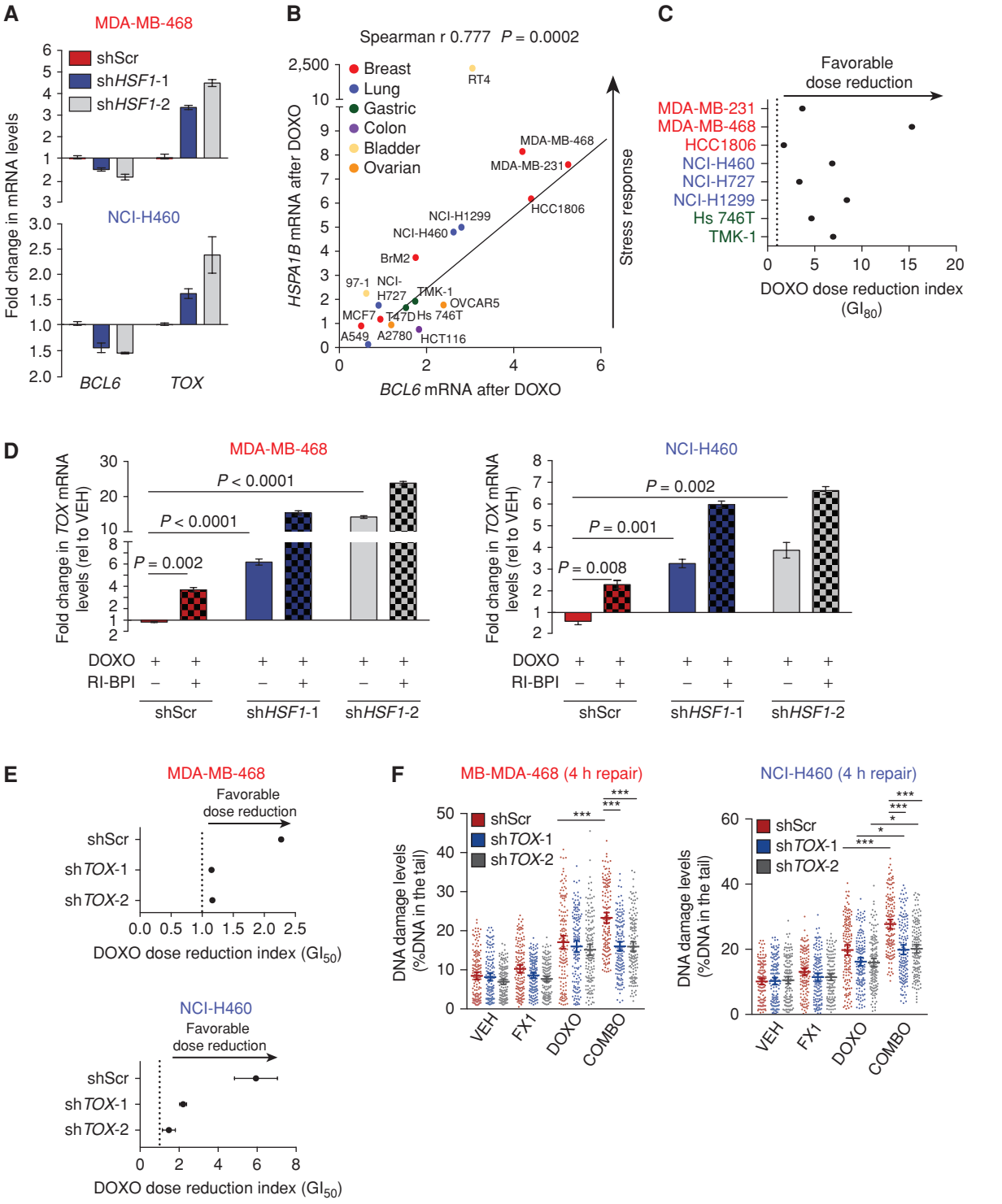

Figure 6. HSF1–BCL6^{BTB}–TOX stress tolerance axis is active in cancer cells and promotes chemoresistance by enhancing DNA repair. **A,** *BCL6* and *TOX* mRNA in MDA-MB-468 and NCI-H460 cells transduced with *HSF1*-targeting shRNAs ($n = 3$ biological replicates). **B,** *BCL6* and *HSPA1B* mRNAs after doxorubicin (DOXO) in cancer cells (representative of at least three biological replicates). **C,** Dose reduction index of RI-BPI and DOXO in solid tumor cell lines (representative of 2–3 biological replicates). **D,** *TOX* expression in doxorubicin-treated MDA-MB-468 (100 nmol/L) and NCI-H460 (200 nmol/L) transduced with *HSF1*-targeting shRNAs and/or treated with 10 μmol/L RI-BPI (representative of three biological replicates). **E,** Dose reduction index of RI-BPI and DOXO of breast cancer cell lines transduced with *TOX*-targeting hairpins (representative of three biological replicates). **F,** Comet assay showing amount of residual DNA damage after 4 hours of repair in TOX-silenced MDA-MB-468 and NCI-H460 cells exposed to 200 nmol/L doxorubicin or 25 μmol/L FX1, alone or in combination (representative of three biological replicates). *, $P < 0.05$; ***, $P < 0.001$.

Published OnlineFirst February 18, 2019; DOI: 10.1158/2159-8290.CD-17-1444

in most cancer cells (Fig. 7A). Furthermore, we found that the combination of FX1 with either doxorubicin (in TNBC cells) or cisplatin (in NSCLC cells) resulted in increased cell-cycle arrest (Fig. 7B; Supplementary Fig. S7A) and enhanced apoptosis compared with either drug alone (Fig. 7C).

To determine whether a similar effect could be observed *in vivo*, we engrafted TNBC (MDA-MB-468) and NSCLC (NCI-H460) cell lines in mice, and when tumors reached 75–100 mm^3, we randomized them into four groups (n = 9–10) to receive doxorubicin (for TNBC), cisplatin (for NSCLC), or respective vehicles, followed by FX1 (or vehicle) according to the schedule shown in Fig. 7D. We measured the tumor volume over time and calculated the AUC for tumor growth. As expected, neither doxorubicin in MDA-MB-468 tumors nor cisplatin in NCI-H460 tumors induced a significant decrease in tumor growth compared with vehicle-treated mice (Fig. 7E; Supplementary Fig. S7B), consistent with these being chemorefractory cells. FX1 alone significantly reduced the tumor growth compared with vehicle-treated mice in both tumor types (Fig. 7E). However, the administration of FX1 in mice receiving either chemotherapy agent decreased the tumor growth to a significantly greater extent than either treatment alone (Fig. 7E). Decreased tumor growth was accompanied with an increase in the abundance of apoptotic cells (Fig. 7F), indicating a reduced tolerance to the cytotoxic agents. The combination of doxorubicin or cisplatin with FX1 was well tolerated, as there was no significant difference in biochemical parameters and body weight of animals treated with the combination with the exception of mild hypokalemia in mice treated with cisplatin and FX1 (Supplementary Fig. S7C; Supplementary Table S1). Taken together, we propose a model where tumor cells take advantage of the HSF1–BCL6 axis to repress *TOX* expression and allow cells to increase their DNA repair capacity, facilitating increased chemotolerance (Supplementary Fig. S8).

DISCUSSION

Herein we explored the mechanism and significance of BCL6 expression in solid tumors. These studies led us to discover an evolutionarily conserved HSF1-BCL6 stress adaptation mechanism in vertebrates, which may explain how natural selection favored development of the BCL6 protein. BCL6 has mostly been thought of in the context of the more recently evolved humoral immune system where it is required for B cells to generate high-affinity antibodies. However, our research points to stress adaptation as a more ancient teleological function. Indeed, whereas potentially nonconserved roles have been attributed to BCL6 in different organisms (e.g., axis symmetry in Xenopus; ref. 42), it appears that adaptation to stress downstream of HSF1 may represent an ancestral function shared across cell types and species. This notion is supported by the fact that this BCL6 function is mediated by the BTB lateral groove, its most highly conserved repression motif. We speculate that this BCL6 stress function may have facilitated the success of vertebrate organisms, which reproduce less abundantly than invertebrates, often must survive for longer periods to propagate, and must preserve complex tissue homeostasis.

This function is taken to extreme lengths in GC B cells, which express high levels of BCL6 and tolerate profound stress during immunoglobulin affinity maturation. The evolution of GCs and the humoral immune response may have become possible as a result of this stress response mechanism. Notably, agnathostomes like lampreys developed a humoral immune system based on different cells and antigen-binding proteins than the jawed vertebrates (43). Yet lamprey B-like cells strongly upregulate BCL6, similar to their gnathostome counterparts (44). Hence, a major implication of our work is that the appearance of BCL6 may have enabled convergent evolution of a humoral immune system in both branches of vertebrates. Our data also suggest that GC B cells incorporated not just BCL6 but also the entire HSF1–BCL6 stress pathway into their basic program by triggering its activation through canonical immune signaling ligands.

Our findings shed light on the role of transcription factors during the stress response and in particular during the acquisition of stress tolerance. The initial response to heat shock relies heavily on the activation of HSPs that protect proteins from thermal denaturation and assist in protein refolding. Accordingly, when the functional capacity of HSP90 is overwhelmed, HSF1 is released from HSP90–HSF1 complexes and initiates the transcriptional response to heat shock. HSF1 target genes thus contribute to the induction of stress tolerance. Here we showed that upregulation of the HSF1 target gene *BCL6* is required to assure full protection from subsequent stress. The importance of BCL6 transcriptional activity during cellular stress is enforced by the implication of nuclear HSP90 in the maintenance of the BCL6 repressor complex activity and effective repression of *TOX*. Ultimately, cellular adaptation to stress and survival is modulated by complex functional relationships between HSP90, HSF1, and BCL6, which influence gene expression.

TOX is a member of the HMG-box family of DNA-binding proteins (45). It is interesting to note that, like BCL6 and HSF1, TOX homologs are also found in lampreys, which may suggest that its role in stress tolerance in mammals may be conserved from lower vertebrates like agnatha. In addition, *TOX* is deleted in 6%–7% of patients with DLBCL profiled in TCGA, suggesting that it is a putative tumor suppressor in a disease where BCL6 is already known to be a frequent oncogene. TOX has been previously described to be required for the development of the CD4 T-cell lineage (46); however, it is not yet clear how TOX mediates its effects. HMG-box proteins bind to chromatin and modify the architecture of DNA. However, recent studies in a T-ALL model suggest that TOX does not bind chromatin and instead inhibits NHEJ by directly binding and suppressing recruitment of Ku70/80 to sites of DNA breaks (41). In contrast, HSF1 has been shown to facilitate DNA repair (both homologous recombination repair and NHEJ) by forming a ternary complex with PARP proteins (47). Our studies provide new insight into the antagonistic roles of HSF1 and TOX in DNA repair processes, because we show that repression of *TOX* by the HSF1–BCL6 axis facilitates repair of DNA damage brought upon by various stressors including chemotoxic agents in NSCLC and TNBC cell lines.

We find that solid tumors arising from diverse cell lineages hijack the conserved HSF1–BCL6 stress tolerance axis to maintain their proliferation and survival at least in part through repression of *TOX*. This proposed mechanism enables tumor cells with high HSF1 to better tolerate exposure

Published OnlineFirst February 18, 2019; DOI: 10.1158/2159-8290.CD-17-1444

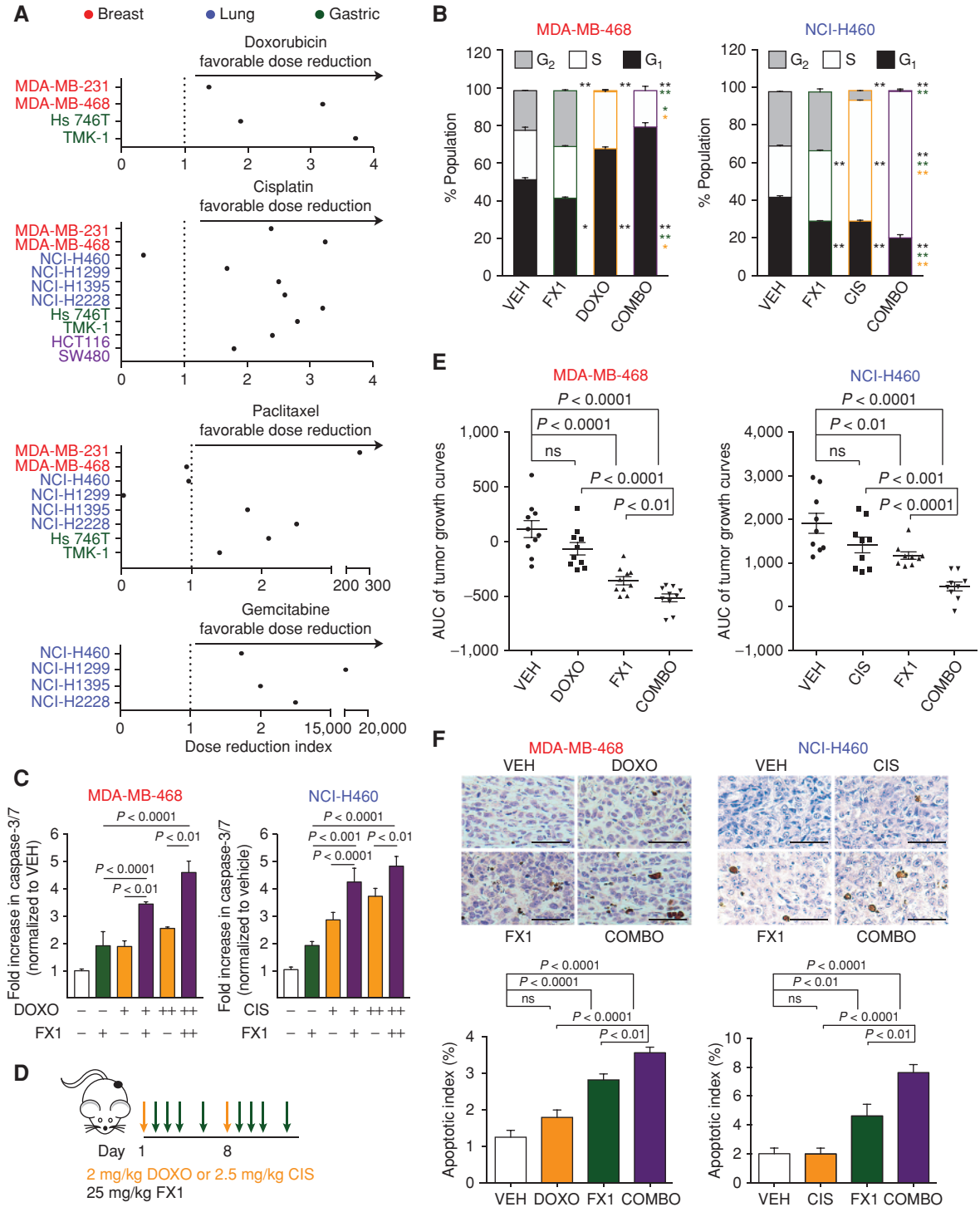

Figure 7. BCL6^{BTB} inhibition overcomes chemotherapy tolerance in cancer cells by inducing apoptosis and cell-cycle arrest. **A,** Dose reduction index of FX1 when combined with doxorubicin (DOXO), cisplatin (CIS), paclitaxel, and gemcitabine in relevant tumor models (doxorubicin: breast, gastric; cisplatin: breast, lung, gastric, and colon; paclitaxel: breast, lung, and gastric; gemcitabine: lung). **B,** Cell-cycle analysis of MDA-MB-468 and NCI-H460 cells exposed to vehicle, 200 nmol/L doxorubicin (MDA-MB-468) or 5.0 μmol/L cisplatin (NCI-H460), 25 μmol/L FX1, or their combination at 24 hours. *, $P < 0.05$; **, $P < 0.01$. Black asterisks represent significance relative to vehicle (VEH) alone; green asterisks represent significance relative to FX1 alone; orange asterisks represent significance relative to doxorubicin/cisplatin alone. **C,** Caspase-3/7 activity in MDA-MB-468 and NCI-H460 cells exposed to vehicle, 100–200 nmol/L doxorubicin (MDA-MB-468) or 2.5–5.0 μmol/L cisplatin (NCI-H460), 25 μmol/L FX1, or their combination (representative of three biological replicates). **D,** Schematic of dosing schedule for xenograft experiments. **E,** Area under the curve (AUC) of the tumor growth curves of MDA-MB-468 and NCI-H460 xenografted mice treated with vehicle, doxorubicin (MDA-MB-468) or cisplatin (NCI-H460), FX1, or their combination ($n = 9$–10 mice per group). **F,** Representative TUNEL staining and quantification of apoptotic index of MDA-MB-468 and NCI-H460 xenografts from **E**. *P* values were calculated by two-sided *t* test. Data presented as mean ± SEM. Scale bars, 100 μm.

Published OnlineFirst February 18, 2019; DOI: 10.1158/2159-8290.CD-17-1444

to additional stressors like chemotherapy. Hence induction of *BCL6* downstream of HSF1 likely supports the ability of cancer cells to endure repeated doses of cytotoxic drugs, potentially allowing the emergence of drug-tolerant persister cells (48). Thus, not surprisingly, patients with high levels of HSF1 and BCL6 fare worse clinically, likely due to the increased fitness of their tumors in response to stress. Conversely, tumors with low HSF1 activity or reduced levels of BCL6 should be unable to adapt to stress and subsequently succumb to the cytotoxic responses induced with repeated dosing of chemotherapy. Therefore pharmacologic inhibition of the HSF1–BCL6 axis might circumvent the incidence of chemotolerance. Therapeutic targeting of the HSF1 stress response pathway has been challenging to date. However, the BCL6–corepressor interface is a druggable target and BCL6 inhibitors may provide the means to deny tumor cells with access to this important stress tolerance mechanism. Combinatorial regimens based on $BCL6^{BTB}$ inhibitors may thus represent a tumor-agnostic form of targeted therapy.

METHODS

Animal Experiments

The maintenance and procedures of all animals were in accordance with and approved by the Research Animal Resource Center of the Weill Cornell Medical College (New York, NY). Mice were sacrificed by CO_2 inhalation followed by cervical dislocation. Mice used for experiments were between 8 and 14 weeks of age. $Hsf1^{+/+}$, $Hsf1^{+/-}$, $Hsf1^{-/-}$, C57BL/6, CBy.SJL(B6)-$Ptprc^a$/J (CD45.1), and $Rag1^{-/-}$ mice were obtained from Jackson Laboratories. SCID mice were obtained from the National Cancer Institute. $Bcl6^{-/-}$ mice were provided by Hilda Ye (Albert Einstein Medical College, New York, NY; ref. 6). $Bcl6^{BTBMUT}$ and $Bcl6^{RD2MUT}$ mice were generated as described previously (36, 37). Mice were selected for experimental groups solely based on genotype. Mice of each genotype were matched as closely as possible for age within constraints of availability. Spleens from $Tox^{-/-}$ mice were provided by Jonathan Kaye (Cedars-Sinai Medical Center, Los Angeles, CA; ref. 46).

GC Formation. Immunologically mature age- and sex-matched $Hsf1^{+/+}$ and $Hsf1^{-/-}$ mice and C57BL/6 mice were immunized intraperitoneally with 0.5 mL 2% SRBCs (Cocalico Biologicals) or a 1:1 mixture of 100 μg of NP-CGG (ratio 20–29, Biosearch Technologies) and alum (Imject alum, Pierce). In time course experiments, mice ($n = 3$ mice per time point) were sacrificed at 48, 72, 120, 144, 168, 192, 216, and 240 hours postimmunization, and in the other experiments mice were sacrificed at day 10.

Heat Stress. $Hsf1^{+/+}$ and $Hsf1^{-/-}$ mice ($n = 2$ per genotype) were anesthetized with a mixture of ketamine 100 mg/kg and xylazine 10 mg/kg intraperitoneally, subjected to nonlethal heat stress for 30 minutes in a 38°C chamber, and sacrificed immediately after.

Mixed Bone Marrow Chimera. For the generation of mixed bone marrow chimera, 4×10^6 cells from a 1:1 mixture of CBy.SJL(B6)-$Ptprc^a$/J bone marrow cells ($CD45.1^+$) and $CD45.2^+$ $Hsf1^{+/+}$ or $Hsf1^{-/-}$ bone marrow cells were injected into the tail veins of sublethally irradiated (400 cGy at 2 doses, 4 hours apart) $Rag1^{-/-}$ mice. Recipient mice were immunized with SRBC 7 weeks later, and GC formation was analyzed 10 days later.

Xenotransplants. Six- to 8-week-old female or male SCID mice housed in a barrier environment were subcutaneously injected in the left flank with 10^7 human breast cancer MDA-MB-468 cells or 10^6 human lung cancer NCI-H460 cells, respectively. Tumor volume was monitored every other day using electronic digital calipers in two dimensions. Tumor volume was calculated using the following formula: tumor volume (mm^3) = (smallest diameter^2 × largest diameter)/2. Then, the AUC was calculated for each individual tumor growth curve to reflect the entire tumor growth (from randomization to sacrifice) and facilitate comparisons among groups (49). When tumors reached a palpable size (approximately 75–100 mm^3), mice were first randomized into two treatment arms ($n = 18$–20 each) to receive either vehicle (water/saline) or chemotherapy (2 mg/kg doxorubicin for MDA-MB-468 and 2.5 mg/kg cisplatin for NCI-H460). On the second day, each arm was further randomized into two arms ($n = 9$–10 each), generating four treatment groups: A, vehicle; B, doxorubicin or cisplatin alone; C, FX1; D, combination of doxorubicin or cisplatin with FX1. Two groups (A and B) received intraperitoneal injections of vehicle (5% Tween-80, 30% PEG-400, 65% dextrose solution 5%) and two groups (C and D) received intraperitoneal injections of 25 mg/kg FX1 according to the schedule shown in Fig. 7D. Mice were weighed twice a week, and liver and kidney chemistry panels were run at sacrifice. All mice were sacrificed when at least 2 tumors out of each group reached 20 mm in any dimension or when they showed signs of severe distress or toxicity.

Thermotolerance Experiments

(i) Thermotolerance of cells grown at 37°C: primary murine splenic $B220^+$ cells, DT40 cells, and IgH-2 cells were left untreated or treated with control or 1 μmol/L RI-BPI peptide. Cells were heat-shocked at 43°C for 1 hour, allowed to recover at 37°C for 12 hours, heat-shocked again at 43°C for 1 hour, and allowed to recover at 37°C for 1 hour. Cell viability was monitored with Trypan blue exclusion or flow cytometry using DAPI exclusion. (ii) Thermotolerance of zebrafish embryos grown at 28°C: 2 ng control morpholino (mo; GeneTools) or bcl6 mo (Open Biosystems) were injected into the yolk of 1–2 cell stage embryos. At 24 hours postfertilization (hpf), embryos were separated into petri dishes and heat-shocked in a water bath at 37°C for 1 hour, allowed to recover at 28°C for 12 hours, heat-shocked again at 37°C for 1 hour, and allowed to recover at 28°C for 12 hours. Zebrafish embryos were counted as nonviable if there was an absence of opaque tissues. Morpholino sequences: control mo: 5′-CCTCCTACCTCAGTTACAATTTATA-3′ and bcl6 mo: 5′-TCTACAAATGAAAATATACCTGGAC-3′. (iii) Thermotolerance of lamprey typhlosole cells grown at 16°C: Cells from lamprey typhlosole were isolated and treated with 1 μmol/L control or RI-BPI peptide. Cells were heat-shocked at 29°C for 1 hour, allowed to recover at 16°C for 12 hours, heat-shocked again at 29°C for 1 hour, and allowed to recover at 16°C for 12 hours. Cell viability was monitored with flow cytometry using DAPI exclusion. (iv) Thermotolerance of *Drosophila* cells grown at 25–26°C: *Drosophila* $S2^+$ cells treated with control or 1 μmol/L RI-BPI peptide were heat-shocked at 37°C for 1 hour, allowed to recover at 25°C for 12 hours, heat-shocked again at 37°C for 1 hour, and allowed to recover at 25°C for 1 hour. Cell viability was monitored with Trypan blue exclusion.

Primary Cell Isolation of Normal Mouse and Human B Cells

Single-cell suspensions of mononuclear cells were generated from murine spleens using red blood cell lysis (Qiagen) or Fico/Lite-LM density gradient media (Atlanta Biologicals). For B220 purification, cells were purified using B220-positive selection or CD43 depletion using the autoMACS cell separation system (Miltenyi Biotec). Splenocytes were determined to be >95% $B220^+$ by flow cytometric analysis. Human IgD^+ NB and $CD77^+$ GC B cells were affinity purified from deidentified human tonsils or spleens using the autoMACS as described previously (50) with approval from the Institutional Review Board of the New York Presbyterian Hospital, Weill Cornell Medical College (New York, NY). NB and GC B-cell purity was determined by flow cytometric analysis to be >90% IgD^+/CD38dim and >90% $CD77^+$/$CD38^{hi}$.

Published OnlineFirst February 18, 2019; DOI: 10.1158/2159-8290.CD-17-1444

Cell Lines

Mammalian. Normal human adult dermal fibroblasts were grown in fibroblast medium supplemented with the serum-free fibroblast growth kit (ATCC). Murine BCL1 cells were grown in RPMI-1640 supplemented with 10% FBS, penicillin G/streptomycin, and 0.05 mmol/L 2-ME. Dog Cf2Th cells were grown in DMEM with 20% FBS, penicillin G/streptomycin, and nonessential amino acids. The bladder cancer cell line RT4 was grown in McCoy 5a medium supplemented with 10% FBS and penicillin G/streptomycin; 97-1 was grown in Ham F-12 medium supplemented with 10% FBS and penicillin G/streptomycin. The breast cancer (HCC1806, MDA-MB-231, MDA-MB-468, MCF7, T47D, BrM2) and colon cancer (HCT116 and SW480) cell lines were grown in DMEM supplemented with 10% FBS and penicillin G/streptomycin. Ovarian cancer cell lines (A2780 and OVCAR5) were grown in RPMI-1640 supplemented with 10% FBS, penicillin G/streptomycin and L-glutamine. The lung cancer cell lines (NCI-H460, NCI-H727, NCI-H1299, NCI-H1395, and NCI-H2228) were grown in DMEM supplemented with 10% FBS, penicillin G/streptomycin, and L-glutamine. Gastric cell lines (Hs 746T and TMK-1) were provided by Dr. Manish A. Shah (Weill Cornell Medicine, New York, NY) and grown in RPMI-1640 supplemented with 10% FBS and penicillin G/streptomycin. All the cell lines were purchased from ATCC unless otherwise stated. Cells were grown in 37°C with 5% CO_2. All cell lines were tested for *Mycoplasma* contamination quarterly by PCR and authenticated once a year using short tandem repeat profiling (Biosynthesis, Inc). Cells were used in experiments within 10–15 passages after thawing.

Nonmammalian. Iguana IgH-2 cells were grown in Eagle Minimum Essential Medium with 10% FBS, penicillin G/streptomycin, L-glutamine, and nonessential amino acids. Chicken DT40 cells were grown in DMEM with 10% FBS, 5% chicken serum, 10% tryptose phosphate broth, penicillin G/streptomycin, and 0.05 mmol/L 2-ME. IgH-2 and DT40 cell lines were obtained from ATCC and used for experiments within 10–15 passages after thawing. Cells were grown at 37°C with 5% CO_2. *Drosophila* $S2^+$ cells were kindly provided by Dr. Eric Lai (Memorial Sloan Kettering Cancer Center, New York, NY) and grown in Schneider's Drosophila medium, 10% FBS, and penicillin G/streptomycin at 25–26°C with ambient CO_2.

Growth Inhibition and DRI Analysis

Cancer cell lines were grown at concentrations sufficient to keep untreated cells in exponential growth over the complete drug exposure time. Cell lines were exposed concurrently to 6 concentrations of RI-BPI (or FX1) and drug for 48–72 hours and analyzed for cell viability using a fluorometric reduction method (CellTiter-Blue, Promega) and/or ATP quantitation (CellTiter-Glo, Promega). Fluorescence ($560_{Ex}/590_{Em}$) or luminescence was determined with the Synergy4 microplate reader (Biotek). The number of viable cells was calculated using the linear least-squares regression of the standard curve. The fluorescence/luminescence was determined for three replicates per treatment condition and normalized to their respective controls (vehicle-treated). CompuSyn software (Biosoft) was used to plot dose–effect curves, determine the drug concentrations that inhibit the growth of the cell lines by 50% and 80% compared with control (GI_{50} and GI_{80}, respectively), and compute the DRI at either the GI_{50} or GI_{80}. The DRI was calculated to quantify the "chemosensitization" effect. The DRI represents how many fold a dose of a drug (e.g., cytotoxic chemotherapy) can be reduced by the addition of another drug (e.g., targeted compound) while maintaining efficacy (51).

Colony-Forming Assay

Solid tumor cell lines were infected with shRNAs and selected for 48 hours with 1 μg/mL puromycin. Cells were counted and plated at 2,000 cells/well (MDA-MB-231 and NCI-H1299) or 200 cells/well (MDA-MB-468, NCI-H460, Hs 746T, and TMK-1) in a 6-well plate. Colonies were allowed to grow for 1–3 weeks until distinct colonies could be visible. Wells were washed with PBS and fixed and stained simultaneously with a 0.1% crystal violet: 20% ethanol solution for 30 minutes at room temperature. Plates were rinsed with water and dried overnight.

DNA Damage by Single-Cell Gel Electrophoresis Assay

Alkaline comet assay was used to assess DNA damage as described previously (52). Cells were exposed to doxorubicin (200 nmol/L) or FX1 (25 μmol/L), alone or in combination, and DNA damage was assessed after 4 hours of continuous exposure and after 4 hours of recovery (where doxorubicin was removed). At each time point, cells were collected, embedded in 0.5% agarose, and lysed overnight at 4°C. Cells were first incubated with alkaline buffer for 40 minutes to unwind the DNA, and then electrophoresis was conducted for 30 minutes. After neutralization, cells were stained with SYBR Green and comets were analyzed within 24 hours. Two slides per condition were imaged for each experiment with an Axiovert 200M fluorescent microscope (Zeiss Inc.), and approximately 50 comets per slide were scored with Comet Score (TriTek).

AlphaLISA HSF1 Reporter Assay

Biotinylated and standard oligonucleotides were purchased from Integrated DNA Technologies (IDT), diluted in Tris-EDTA buffer (pH 8.0), and annealed. Cells were treated [heat shocked for 15 minutes at 43°C (HS) or treated for 1 hour with 500 ng/mL CD40 ligand, 100 ng/mL IL4, or 100 ng/mL IL21] and nuclear extracts were prepared using the Nuclear Extraction kit (Active Motif). For the entire assay, solutions were diluted to their working concentrations in AlphaLISA Immunoassay buffer solution 5X (AL001F). Protein A acceptor beads (6760137, PerkinElmer) were incubated with polyclonal rabbit HSF1 antibody (ADI-SPA-901, Enzo Life Sciences) for 1 hour at room temperature with agitation. Streptavidin donor beads (6760002, PerkinElmer) were added and the mixture was kept in the dark with agitation. Meanwhile, 2 μg of nuclear extract were incubated with annealed biotinylated *HSPA1A* HSE or mutated HSE for 30 minutes in white 384-well Optiplates (6005620, PerkinElmer). A mixture of acceptor and donor beads was added to each well and incubated for 1 hour. Luminescence was measured in an EnVision Multilabel Plate Reader (PerkinElmer).

Fluorescence Polarization Assay

Recombinant HSF1 (rHSF1) was purchased from Enzo (ADI-SPP-900). The fluorescein-dT-labeled oligonucleotides were from IDT. The synthesized probes were 5′-TCGAC/iFluorT/AGAAGCTTCTA GAAGCTTCTAG-3′ (HSPA1A-HSE) and 5′-CCGGCCTTTCCTA GAAACTTCT/iFluorT/GCATC-3′ (BCL6-HSE2). Oligonucleotides were annealed in 100 μmol/L TE (10 mmol/L Tris; 1 mmol/L EDTA; pH 8.0) by incubating at 95°C for 10 minutes followed by cooling to room temperature. Fluorescence polarization (FP; $485_{Ex}/528_{Em}$) was determined for 5 nmol/L of probe in the presence of increasing concentrations of rHSF1 (up to 500 nmol/L) in a Synergy Neo (BioTek) plate reader. Measurement of FP change as a function of protein concentration resulted in a binding isotherm, which was used to determine the dissociation constant for the rHSF1–DNA complex.

HSF1 Chromatin Immunoprecipitation

Chromatin immunoprecipitation (ChIP) was performed as described previously (53). Briefly, NB and GC B cells or solid tumor cell lines were fixed with 1% formaldehyde for 10 minutes at room temperature, quenched with 125 mmol/L glycine, and lysed in modified RIPA buffer (150 mmol/L NaCl, 1% v/v Nonidet P-40, 0.5% w/v deoxycholate, 0.1% w/v SDS, 50 mmol/L Tris pH 8, 5 mmol/L EDTA) supplemented with protease inhibitors. Cell lysates were sonicated

Published OnlineFirst February 18, 2019; DOI: 10.1158/2159-8290.CD-17-1444

using the Branson tip sonicator (Branson) to generate fragments less than 400 bp. Precleared lysates were incubated overnight with 5 μg anti-HSF1 (ADI-SPA-901, Enzo Life Sciences) or control IgG antibody. Immunocomplexes were recovered, sequentially washed with increasing stringency of wash buffers (150 mmol/L NaCl, 250 mmol/L NaCl, 250 mmol/L LiCl), and eluted with 1% SDS and 100 mmol/L $NaHCO_3$. Cross-links were reversed and DNA was purified using a Qiaquick PCR Purification Kit (Qiagen). ChIP DNA was amplified with real-time qPCR using primer sequences in Supplementary Table S2 (IDT), SYBR Green (Quanta Biosciences) on the 7900HT Fast Real-Time PCR System (Applied Biosystems). Input standard curves were used for estimation of relative enrichment.

Nascent RNA Capture Assay

Murine $B220^+$ splenocytes or human cells transfected using Lipofectamine 2000 (Invitrogen) with 50 nmol/L siRNAs targeting *HSF1* (Hs_HSF1_6: 5′-GCUUCGUGCGGCAGCUCAATT-3′, Hs_HSF1_9: 5′-GGUUGUUCAUAGUCAGAAUTT-3′, Qiagen) or a nontargeting control (Stealth RNAi medium GC duplex, Invitrogen) for 48 hours were heat shocked at 43°C for 2 hours followed by recovery at 37°C for 2 hours while simultaneously pulsed with 0.2 mmol/L ethynyl uridine (EU). EU-labeled RNA was captured with the Click-It Nascent RNA capture kit (Molecular Probes). Briefly, RNA was biotinylated, conjugated to streptavidin beads, and converted to cDNA using the SuperScript III first-strand synthesis system (Invitrogen). A fraction of the undiluted cDNA was used in the qPCR and detected by fast SYBR Green (Quanta Biosciences) on the 7900HT Fast Real-Time PCR System (Applied Biosystems).

Statistical Analysis

Unless specified, we reported the mean and SEM and *P* values associated with a Student *t* test with two-tailed distribution of equal variance (or nonparametric equivalent test when appropriate) for experimental data. *P* values < 0.05 were considered statistically significant. No statistical methods were used to predetermine sample size and no samples were excluded specifically from the analysis.

Data Deposition

The data from the mRNA-seq experiments were deposited in GEO database under accession GSE69974.

Survival analysis, QPCR, mRNA sequencing, immunofluorescence, immunohistology and imaging analysis, flow cytometry, enzyme-linked immunosorbent assay, immunoblots, protein sequence variability analysis, lentiviral transduction, caspase-3/7 activity, and compounds are described in Supplementary Materials.

Disclosure of Potential Conflicts of Interest

A.M. Melnick reports receiving a commercial research grant from Janssen and is a consultant/advisory board member for the same. No potential conflicts of interest were disclosed by the other authors.

Authors' Contributions

Conception and design: T.M. Fernando, R. Marullo, A.M. Melnick, L. Cerchietti
Development of methodology: R. Marullo, B. Pera Gresely, J.M. Phillip, M. Hirano, A.M. Melnick, L. Cerchietti
Acquisition of data (provided animals, acquired and managed patients, provided facilities, etc.): T.M. Fernando, R. Marullo, S.N. Yang, G. Lundell-Smith, I. Torregroza, H. Ahn, T. Evans, G.G. Privé, M. Hirano, A.M. Melnick, L. Cerchietti
Analysis and interpretation of data (e.g., statistical analysis, biostatistics, computational analysis): T.M. Fernando, R. Marullo, B. Pera Gresely, J.M. Phillip, S.N. Yang, G. Lundell-Smith, H. Ahn, T. Evans, B. Győrffy, G.G. Privé, A.M. Melnick, L. Cerchietti
Writing, review, and/or revision of the manuscript: T.M. Fernando, R. Marullo, T. Evans, B. Győrffy, G.G. Privé, A.M. Melnick, L. Cerchietti
Administrative, technical, or material support (i.e., reporting or organizing data, constructing databases): M. Hirano, A.M. Melnick
Study supervision: A.M. Melnick, L. Cerchietti

Acknowledgments

Bcl6-null mice were provided by Hilda Ye (Albert Einstein Medical College, New York, NY). Spleens from Tox-null mice were provided by Jonathan Kaye (Cedars-Sinai Medical Center, Los Angeles, CA). We thank the Memorial Sloan Kettering Cancer Center Translational Core for technical assistance with bone marrow experiments and the Weill Cornell Epigenomics Core for high-throughput data processing. This work was supported by NIH grants F31CA167999 (to T.M. Fernando), R01AI072435 (to M. Hirano), R01GM100151 (to M. Hirano), NSF1655163 (to M. Hirano), NSF1755418 (to M. Hirano), R01HL111400 (to T. Evans), R01CA155226 (to A. Melnick), R35CA220499 (to A. Melnick), and P50CA192937 (to A. Melnick). L. Cerchietti was supported by the American Society of Hematology Scholar Award. A. Melnick is also supported by the Chemotherapy Foundation and the Follicular Lymphoma Consortium. R. Marullo is supported by a grant from the Lung Cancer Research Foundation. G.G. Privé was supported by grants from the CCSRI, CRS, CIHR, and the Waxman Foundation.

The costs of publication of this article were defrayed in part by the payment of page charges. This article must therefore be hereby marked *advertisement* in accordance with 18 U.S.C. Section 1734 solely to indicate this fact.

Received December 22, 2017; revised November 19, 2018; accepted February 13, 2019; published first February 18, 2019.

REFERENCES

1. Hatzi K, Melnick A. Breaking bad in the germinal center: how deregulation of BCL6 contributes to lymphomagenesis. Trends Mol Med 2014;20:343–52.
2. Walker SR, Liu S, Xiang M, Nicolais M, Hatzi K, Giannopoulou E, et al. The transcriptional modulator BCL6 as a molecular target for breast cancer therapy. Oncogene 2015;34:1073–82.
3. Deb D, Rajaram S, Larsen JE, Dospoy PD, Marullo R, Li LS, et al. Combination therapy targeting BCL6 and phospho-STAT3 defeats intratumor heterogeneity in a subset of non-small cell lung cancers. Cancer Res 2017;77:3070–81.
4. Xu L, Chen Y, Dutra-Clarke M, Mayakonda A, Hazawa M, Savinoff SE, et al. BCL6 promotes glioma and serves as a therapeutic target. Proc Natl Acad Sci U S A 2017;114:3981–6.
5. Dent AL, Shaffer AL, Yu X, Allman D, Staudt LM. Control of inflammation, cytokine expression, and germinal center formation by BCL-6. Science 1997;276:589–92.
6. Ye BH, Cattoretti G, Shen Q, Zhang J, Hawe N, de Waard R, et al. The BCL-6 proto-oncogene controls germinal-centre formation and Th2-type inflammation. Nat Genet 1997;16:161–70.
7. Fukuda T, Yoshida T, Okada S, Hatano M, Miki T, Ishibashi K, et al. Disruption of the Bcl6 gene results in an impaired germinal center formation. J Exp Med 1997;186:439–48.
8. Cerchietti LC, Lopes EC, Yang SN, Hatzi K, Bunting KL, Tsikitas LA, et al. A purine scaffold Hsp90 inhibitor destabilizes BCL-6 and has specific antitumor activity in BCL-6-dependent B cell lymphomas. Nat Med 2009;15:1369–76.
9. Akerfelt M, Morimoto RI, Sistonen L. Heat shock factors: integrators of cell stress, development and lifespan. Nat Rev Mol Cell Biol 2010;11:545–55.
10. Whitesell L, Lindquist S. Inhibiting the transcription factor HSF1 as an anticancer strategy. Expert Opin Ther Targets 2009;13:469–78.

11. Jolly C, Morimoto RI. Role of the heat shock response and molecular chaperones in oncogenesis and cell death. J Natl Cancer Inst 2000;92:1564–72.
12. Tang D, Khaleque MA, Jones EL, Theriault JR, Li C, Wong WH, et al. Expression of heat shock proteins and heat shock protein messenger ribonucleic acid in human prostate carcinoma in vitro and in tumors in vivo. Cell Stress Chaperones 2005;10:46–58.
13. Zaarur N, Gabai VL, Porco JA Jr, Calderwood S, Sherman MY. Targeting heat shock response to sensitize cancer cells to proteasome and Hsp90 inhibitors. Cancer Res 2006;66:1783–91.
14. Dai C, Santagata S, Tang Z, Shi J, Cao J, Kwon H, et al. Loss of tumor suppressor NF1 activates HSF1 to promote carcinogenesis. J Clin Invest 2012;122:3742–54.
15. Dai C, Whitesell L, Rogers AB, Lindquist S. Heat shock factor 1 is a powerful multifaceted modifier of carcinogenesis. Cell 2007;130:1005–18.
16. Zhao Y, Liu H, Liu Z, Ding Y, Ledoux SP, Wilson GL, et al. Overcoming trastuzumab resistance in breast cancer by targeting dysregulated glucose metabolism. Cancer Res 2011;71:4585–97.
17. Jin X, Moskophidis D, Mivechi NF. Heat shock transcription factor 1 is a key determinant of HCC development by regulating hepatic steatosis and metabolic syndrome. Cell Metab 2011;14:91–103.
18. Min JN, Huang L, Zimonjic DB, Moskophidis D, Mivechi NF. Selective suppression of lymphomas by functional loss of Hsf1 in a p53-deficient mouse model for spontaneous tumors. Oncogene 2007;26:5086–97.
19. Khaleque M, Bharti A, Gong J, Gray PJ, Sachdev V, Ciocca DR, et al. Heat shock factor 1 represses estrogen-dependent transcription through association with MTA1. Oncogene 2008;27:1886–93.
20. Meng L, Gabai VL, Sherman MY. Heat-shock transcription factor HSF1 has a critical role in human epidermal growth factor receptor-2-induced cellular transformation and tumorigenesis. Oncogene 2010;29:5204–13.
21. Fang F, Chang R, Yang L. Heat shock factor 1 promotes invasion and metastasis of hepatocellular carcinoma *in vitro* and *in vivo*. Cancer 2012;118:1782–94.
22. Mendillo ML, Santagata S, Koeva M, Bell GW, Hu R, Tamimi RM, et al. HSF1 drives a transcriptional program distinct from heat shock to support highly malignant human cancers. Cell 2012;150:549–62.
23. Santagata S, Hu R, Lin NU, Mendillo ML, Collins LC, Hankinson SE, et al. High levels of nuclear heat-shock factor 1 (HSF1) are associated with poor prognosis in breast cancer. Proc Natl Acad Sci U S A 2011;108:18378–83.
24. McMillan DR, Xiao X, Shao L, Graves K, Benjamin IJ. Targeted disruption of heat shock transcription factor 1 abolishes thermotolerance and protection against heat-inducible apoptosis. J Biol Chem 1998;273:7523–8.
25. Xiao X, Zuo X, Davis AA, McMillan DR, Curry BB, Richardson JA, et al. HSF1 is required for extra-embryonic development, postnatal growth and protection during inflammatory responses in mice. EMBO J 1999;18:5943–52.
26. Cattoretti G, Chang CC, Cechova K, Zhang J, Ye BH, Falini B, et al. BCL-6 protein is expressed in germinal-center B cells. Blood 1995;86:45–53.
27. Onizuka T, Moriyama M, Yamochi T, Kuroda T, Kazama A, Kanazawa N, et al. BCL-6 gene product, a 92- to 98-kD nuclear phosphoprotein, is highly expressed in germinal center B cells and their neoplastic counterparts. Blood 1995;86:28–37.
28. Guettouche T, Boellmann F, Lane WS, Voellmy R. Analysis of phosphorylation of human heat shock factor 1 in cells experiencing a stress. BMC Biochem 2005;6:4.
29. Zotos D, Coquet JM, Zhang Y, Light A, D'Costa K, Kallies A, et al. IL-21 regulates germinal center B cell differentiation and proliferation through a B cell-intrinsic mechanism. J Exp Med 2010;207:365–78.
30. Liu D, Xu H, Shih C, Wan Z, Ma X, Ma W, et al. T-B-cell entanglement and ICOSL-driven feed-forward regulation of germinal centre reaction. Nature 2015;517:214–8.
31. Inouye S, Izu H, Takaki E, Suzuki H, Shirai M, Yokota Y, et al. Impaired IgG production in mice deficient for heat shock transcription factor 1. J Biol Chem 2004;279:38701–9.
32. Johnston RJ, Poholek AC, DiToro D, Yusuf I, Eto D, Barnett B, et al. Bcl6 and Blimp-1 are reciprocal and antagonistic regulators of T follicular helper cell differentiation. Science 2009;325:1006–10.
33. Nurieva RI, Chung Y, Martinez GJ, Yang XO, Tanaka S, Matskevitch TD, et al. Bcl6 mediates the development of T follicular helper cells. Science 2009;325:1001–5.
34. Yu D, Rao S, Tsai LM, Lee SK, He Y, Sutcliffe EL, et al. The transcriptional repressor Bcl-6 directs T follicular helper cell lineage commitment. Immunity 2009;31:457–68.
35. Ying CY, Dominguez-Sola D, Fabi M, Lorenz IC, Hussein S, Bansal M, et al. MEF2B mutations lead to deregulated expression of the oncogene BCL6 in diffuse large B cell lymphoma. Nat Immunol 2013;14:1084–92.
36. Huang C, Hatzi K, Melnick A. Lineage-specific functions of Bcl-6 in immunity and inflammation are mediated by distinct biochemical mechanisms. Nat Immunol 2013;14:380–8.
37. Huang C, Gonzalez DG, Cote CM, Jiang Y, Hatzi K, Teater M, et al. The BCL6 RD2 domain governs commitment of activated B cells to form germinal centers. Cell Rep 2014;8:1497–508.
38. Cerchietti LC, Yang SN, Shaknovich R, Hatzi K, Polo JM, Chadburn A, et al. A peptomimetic inhibitor of BCL6 with potent antilymphoma effects *in vitro* and *in vivo*. Blood 2009;113:3397–405.
39. Vydra N, Toma A, Widlak W. Pleiotropic role of HSF1 in neoplastic transformation. Curr Cancer Drug Targets 2014;14:144–55.
40. Cardenas MG, Yu W, Beguelin W, Teater MR, Geng H, Goldstein RL, et al. Rationally designed BCL6 inhibitors target activated B cell diffuse large B cell lymphoma. J Clin Invest 2016;126:3351–62.
41. Lobbardi R, Pinder J, Martinez-Pastor B, Theodorou M, Blackburn JS, Abraham BJ, et al. TOX regulates growth, DNA repair, and genomic instability in T-cell acute lymphoblastic leukemia. Cancer Discov 2017;7:1336–53.
42. Sakano D, Kato A, Parikh N, McKnight K, Terry D, Stefanovic B, et al. BCL6 canalizes Notch-dependent transcription, excluding Mastermind-like1 from selected target genes during left-right patterning. Dev Cell 2010;18:450–62.
43. Boehm T, McCurley N, Sutoh Y, Schorpp M, Kasahara M, Cooper MD. VLR-based adaptive immunity. Annu Rev Immunol 2012;30:203–20.
44. Hirano M, Guo P, McCurley N, Schorpp M, Das S, Boehm T, et al. Evolutionary implications of a third lymphocyte lineage in lampreys. Nature 2013;501:435–8.
45. O'Flaherty E, Kaye J. TOX defines a conserved subfamily of HMG-box proteins. BMC Genomics 2003;4:13.
46. Aliahmad P, Kaye J. Development of all CD4 T lineages requires nuclear factor TOX. J Exp Med 2008;205:245–56.
47. Fujimoto M, Takii R, Takaki E, Katiyar A, Nakato R, Shirahige K, et al. The HSF1-PARP13-PARP1 complex facilitates DNA repair and promotes mammary tumorigenesis. Nat Commun 2017;8:1638.
48. Sharma SV, Lee DY, Li B, Quinlan MP, Takahashi F, Maheswaran S, et al. A chromatin-mediated reversible drug-tolerant state in cancer cell subpopulations. Cell 2010;141:69–80.
49. Duan F, Simeone S, Wu R, Grady J, Mandoiu I, Srivastava PK. Area under the curve as a tool to measure kinetics of tumor growth in experimental animals. J Immunol Methods 2012;382:224–8.
50. Ci W, Polo JM, Cerchietti L, Shaknovich R, Wang L, Yang SN, et al. The BCL6 transcriptional program features repression of multiple oncogenes in primary B cells and is deregulated in DLBCL. Blood 2009;113:5536–48.
51. Chou TC. Theoretical basis, experimental design, and computerized simulation of synergism and antagonism in drug combination studies. Pharmacol Rev 2006;58:621–81.
52. Marullo R, Werner E, Zhang H, Chen GZ, Shin DM, Doetsch PW. HPV16 E6 and E7 proteins induce a chronic oxidative stress response via NOX2 that causes genomic instability and increased susceptibility to DNA damage in head and neck cancer cells. Carcinogenesis 2015;36:1397–406.
53. Hatzi K, Jiang Y, Huang C, Garrett-Bakelman F, Gearhart MD, Giannopoulou EG, et al. A hybrid mechanism of action for BCL6 in B cells defined by formation of functionally distinct complexes at enhancers and promoters. Cell Rep 2013;4:578–88.

Published OnlineFirst February 18, 2019; DOI: 10.1158/2159-8290.CD-17-1444

AACR American Association for Cancer Research

CANCER DISCOVERY

BCL6 Evolved to Enable Stress Tolerance in Vertebrates and Is Broadly Required by Cancer Cells to Adapt to Stress

Tharu M. Fernando, Rossella Marullo, Benet Pera Gresely, et al.

Cancer Discov 2019;9:662-679. Published OnlineFirst February 18, 2019.